



**Numerical Simulation of the Performance of Sb_2Se_3 Solar Cell via Optimizing the
Optoelectronic Properties based on SCAPS-1D.**

Saraswati Bajgai

**Thesis Submitted in Fulfilment of the Requirements for the Degree of
Master of Science in Sustainable Energy Management
(Internation Program)
Prince of Songkla University**

2023

Copyright of Prince of Songkla University



**Numerical Simulation of the Performance of Sb_2Se_3 Solar Cell via Optimizing the
Optoelectronic Properties based on SCAPS-1D.**

Saraswati Bajgai

**Thesis Submitted in Fulfilment of the Requirements for the Degree of
Master of Science in Sustainable Energy Management
(Internation Program)
Prince of Songkla University**

2023

Copyright of Prince of Songkla University

Thesis Title Numerical Simulation of the Performance of Sb₂Se₃ Solar Cell via Optimizing the Optoelectronic Properties based on SCAPS-1D
Author Saraswati Bajgai
Major Program Sustainable Energy Management

Major Advisor




 (Assoc. Prof. Dr. Kuaanan Techato)


Examining Committee:


 Chairperson
 (Dr. Mohammad Shah Jamal)


Committee
 (Assoc. Prof. Dr. Kuaanan Techato)


Committee
 (Asst. Prof. Dr. Montri Luengchavanon)



 Committee
 (Assoc. Prof. Dr. Khamphe Phoungthong)



Committee
 (Dr. Nuttaya Yuangyai)

The Graduate School, Prince of Songkla University, has approved this thesis as fulfillment of the requirements for the Master of Sustainable Energy Management.


.....
 (Asst. Prof. Dr. Thakerng Wongsirichot)
 Acting Dean of Graduate School

This is to certify that the work here submitted is the result of the candidate's own investigations. Due acknowledgement has been made of any assistance received.

..........Signature
(Assoc. Prof. Dr. Kuaanan Techato)
Major Advisor

..........Signature
(Ms. Saraswati Bajgai)
Candidate

I hereby certify that this work has not been accepted in substance for any other degree and is not being currently submitted in candidature for any degree.


.....Signature

(Ms. Saraswati Bajgai)

Candidate

| | |
|----------------------|--|
| Thesis Title | Numerical Simulation of the Performance of Sb ₂ Se ₃ Solar Cell via Optimizing the Optoelectronic Properties based on SCAPS-1D |
| Author | Saraswati Bajgai |
| Major Program | Sustainable Energy Management |
| Academic Year | 2022 |

ABSTRACT

The study analyzed the potential of using antimony selenide (Sb₂Se₃) as a material for solar cells by conducting simulations using the Solar Cell Capacitance Simulator (SCAPS) program. The non-toxic and accessible nature of Sb₂Se₃, coupled with its potential for high efficiency and low cost, makes it an exciting material for the future of solar cell technology. The analysis focused on various factors, including the thickness of the Sb₂Se₃ layer, its defect density, band gap, energy level, and carrier concentration, and their influence on the performance of the solar cells. The simulation results indicated that an optimal performance of the devices could be achieved with specific values for the Sb₂Se₃ layer: an 800nm thickness for the absorber, a defect density less than 10¹⁵ cm⁻³, a band gap of 1.2 eV, an energy level of 0.1 eV (above the valence band), and a carrier concentration of 10¹⁴ cm⁻³. By optimizing these parameters, a maximum efficiency of 30% was attained. Overall, the study's findings offer valuable insights and directions for designing and engineering solar cells using Sb₂Se₃ as a material.

ACKNOWLEDGEMENT

I would like to express my gratitude to my parents and siblings for shaping who I am today. Their unwavering support and assistance have been indispensable to the success of this endeavor, and I sincerely appreciate everything they have done for me. I am thankful to Associate Professor Dr. Kuaanan Techato for his advice and support, which made working on this research more exciting and productive. I would also like to express my gratitude to Mr. Shahriar Chowdary, my co-advisor, for his constant encouragement and support throughout the composition of my thesis. His unending encouragement and enthusiasm pushed me throughout the course. Finally, I would like to thank Miss Sutawan for her unwavering support."

I would like to thank Prince of Songkla University for providing me the opportunity to study and supporting with the grants for research studies. Additionally, I would like to thank Ghent University, Belgium for providing us with the SCAPS 1-D software to run the simulation. Also, the Institute of Fuel Research and Development (IFRD), Bangladesh Council of Scientific and Industrial Research (BCSIR), Dhaka 1205, Bangladesh

Saraswati Bajgai

CONTENT

| CONTENTS | PAGE |
|--------------------------------------|----------|
| ABSTRACT | V |
| ACKNOWLEDGEMENT | VI |
| CONTENT | VII-IX |
| LIST OF TABLES | X |
| LIST OF FIGURES | XI-XII |
| LIST OF ABBREVIATIONS AND SYMBOLS | XIII-XIV |
| CHAPTER 1 | 1 |
| INTRODUCTION | 1 |
| 1.1 Background | 1-4 |
| 1.2 Problem Statement | 4 |
| 1.3 The research questions | 4-5 |
| 1.4 Research Objectives | 5 |
| 1.5 Research Scope | 5 |
| CHAPTER 2 | 6 |
| LITERATURE REVIEW | 6 |
| 2.1 Renewable energy | 6-8 |
| 2.2 Solar PV Technology Installation | 9 |

| | |
|--|-------|
| 2.3 Solar energy | 10-14 |
| • Solar cell | 10-11 |
| ➤ First generation | 12 |
| ➤ Second generation | 12-13 |
| ➤ Third generation | 13-14 |
| 2.4 Perovskite Solar Cell | 14-18 |
| 2.5 Antimony Selenide(Sb_2Se_3) | 18-21 |
| 2.5.1 Antimony selenide structures | 21-29 |
| ➤ Mesoporous sensitized structure | 26 |
| ➤ Planar Structure | 27-28 |
| ➤ Superstrate planar structure | 28-29 |
| 2.5.2 Present status of Antimony Selenide Solar Cells | 29-31 |
| 2.6 Solar cells simulators and current-voltage measurement | 32-38 |
| • Band gap | 32-34 |
| • Short circuit current (I_{sc}) | 34-35 |
| • Open circuit voltage (V_{oc}) and Closed-circuit voltage | 35-36 |
| • Quantum efficiency and Efficiency Value | 38 |
| CHAPTER 3 | 39 |
| RESEARCH METHODOLOGY | 39 |
| 3.1 Materials | 39 |
| 3.1.1. Simulation Parameters | 39-41 |
| 3.1.2 Numerical Simulation Method | 41-43 |

| | |
|---|-------|
| CHAPTER 4 | 44 |
| RESULTS AND DISCUSSION | 44 |
| 4.1 Effect of absorber layer thickness with QE | 44-45 |
| 4.2 Effect of absorber layer Carrier concentration and bandgap | 45-47 |
| 4.3 Defect density vs energy level | 47-49 |
| 4.4 Effect of defect density of the absorption layer on the PSC performance | 49-51 |
| 4.5 Effect of the interface defect density on the PSC performance | 51-52 |
| 4.6 Effect of electron affinity with bandgap | 52-54 |
| CHAPTER 4 | 55 |
| CONCLUSION AND FUTURE PROSPECTS | 55-56 |
| REFERENCES | 57-71 |
| VITAE | 72 |

LIST OF TABLES**Table**

| | | |
|---------|--|-------|
| Table 1 | The literature-report of photovoltaic capabilities of HTL-free antimony trisulfide solar cells along with absorber deposition techniques | 24 |
| Table 2 | The performances of Sb ₂ S ₃ solar cells based on organic HTLs, as well as absorber deposition techniques | 25 |
| Table 3 | List of various simulation parameters involved in the perovskite planar structure | 40-41 |

LIST OF FIGURES

Figure

| | | |
|-----------|---|----|
| Figure 1 | The share of modern renewable energy | 7 |
| Figure 2 | The net renewable energy production between 2019 and 2021 | 8 |
| Figure 3 | The overall amount of installed renewable power generation | 9 |
| Figure 4 | Classification of solar photovoltaic cells generation | 11 |
| Figure 5 | Molecular structure of Perovskite solar cell showing A, B and x | 14 |
| Figure 6 | The device structure of a perovskite solar cell | 15 |
| Figure 7 | Crystal diagram of Antimony selenide | 19 |
| Figure 8 | Schematic of the Sb_2Se_3 solar cell | 20 |
| Figure 9 | Schematic representations of three common Sb_2Se_3 solar cell device architectures: (a) mesoporous sensitized structure; (b) Substrate planar structure; and (c) Superstrate planar structure | 27 |
| Figure 10 | Displays sensitized solar cells and planar solar cells | 28 |
| Figure 11 | The significant developments in antimony chalcogenide solar cells | 31 |
| Figure 12 | The density of states | 33 |
| Figure 13 | The current-voltage characteristics of a solar cell | 34 |
| Figure 14 | The illustration of closed and open circuit | 35 |
| Figure 15 | Circuit diagram of a PV cell | 37 |
| Figure 16 | Structure of the Sb_2Se_3 solar cell device | 39 |
| Figure 17 | Absorber layer thickness with a) V_{oc} & FF, b) J_{sc} & Efficiency, c) Quantum Efficiency | 45 |

| | | |
|-----------|--|----|
| Figure 18 | Photovoltaic performance parameters at various carrier concentrations | 47 |
| Figure 19 | Photovoltaic performance parameters at various defect density | 49 |
| Figure 20 | Performance of the PSC as a function of parameters like absorber defect density and layer thickness shown using contour graphs | 51 |
| Figure 21 | contour graphs to show the PSC performance in relation to different parameters of the Antimony Triselenide Layer | 52 |
| Figure 22 | Effect of electron affinity with bandgap | 54 |

LIST OF ABBREVIATIONS

| | |
|---------------------------------|--|
| GHG | Greenhouse gas |
| EJ | Exajoule |
| a-Si | Amorphous silicon |
| CdTe | Cadmium telluride |
| CIS | Copper indium selenide |
| HTL | Hole transport layer |
| ETL | Electron hole layer |
| ITO | Indium tin oxide |
| FTO | Fluorine-doped Tin Oxide |
| DSSC | Dye sensitized solar cell. |
| SCAPS 1-D | Cell Capacitance Simulator |
| PV technology | Solar Photovoltaic technology |
| Sb ₂ Se ₃ | Antimony selenide |
| AM 1.5 | Reference global spectrums at air mass 1.5 |
| CBM | Conduction band minimum |
| mpp | Maximum power point |
| V _{mpp} | Maximum power point voltage |
| PCE | Power conversion efficiency |
| CZTS | Copper zinc tin selenide |
| SnS | Tin silfide |
| Cu ₂ O | Copper (I) oxide or cuprous oxide |

| | |
|------------------|-----------------------|
| ZnO | Zinc oxide |
| TiO ₂ | Titanium dioxide |
| I _{sc} | Short circuit Current |
| V _{oc} | Open circuit voltage |
| J _{sc} | Current density |
| FF | Fill Factor |

CHAPTER 1

INTRODUCTION

1.1. Background and rationale

Solar energy can be harnessed to fulfil expanding energy requirements. The increased use of solar energy necessitates the development of novel photovoltaic (PV) technologies with low manufacturing costs and high power conversion efficiencies (PCE)[2]. Thin-film photovoltaic (TFPV) technologies have drawn huge research focus due to the benefits of lesser material consumption, greater power production, and scalable flexibility [3-5]. For the different types of thin-film solar cells, notable successes have been attained in the representative cadmium telluride (CdTe)[6], copper indium gallium selenide (CIGS) [7, 8], and perovskites [9]. The scarcity of indium (In) and the toxicity of cadmium (Cd) limit their long-term use. Therefore, various low-toxic and earth-abundant photo absorber materials, such as CZTS, SnS, Cu₂O, CuSbSe₂, and Sb₂Se₃, have been explored for photovoltaic (PV) applications [10, 11]. Among the chalcogenide family of materials, antimony selenide (Sb₂Se₃) has emerged as a potential candidate for the next generation of light-harvesting materials due to its high absorption coefficients ($>10^5 \text{ cm}^{-1}$), suitable band-gap energy of 1.1–1.2 eV, and earth-abundant and low-toxic constituents [12, 13].

Sb₂Se₃ has garnered considerable interest in recent years due to its excellent photo conducting properties and superior thermoelectric power [14] making it useful for optical and thermoelectric cooling applications. In addition to these uses, Sb₂Se₃ has diverse applications in photodetectors, solar cells, batteries, and memory devices [15]. All these applications depend heavily on the electrical, optical, microstructural, and other properties of Sb₂Se₃. Material synthesis and deposition also play a crucial role in achieving high-quality materials. In the past decade, Sb₂Se₃ solar cells have been extensively studied, resulting in significant advancements with power conversion efficiencies (PCEs) of 3.21%, 7.6%, and 9.2% [3]. Antimony chalcogenide solar cells have seen performance improvements due to several factors. Advanced growth techniques like vapor transport deposition and hydrothermal have

improved the quality and uniformity of the absorber layer, resulting in higher efficiency [16]. Buffer layer optimization with CdTe, ZnO, and TiO₂ has improved device stability and prevented absorber layer defects. Innovative device designs have also played a role. The photovoltage of Sb₂Se₃ cells is low, but improved hole transport layers can overcome this. The HTL is an essential component of the solar cell that helps to transport holes (positively charged carriers) from the absorber layer to the anode. By optimizing the HTL, researchers have been able to improve the overall device performance of antimony chalcogenide solar cells [17].

Chen et al. (2017) reported that the efficiency of Sb₂Se₃ cells was improved from 5.42% to 6.50% by incorporating an inorganic PbS colloidal quantum dot film [18]. Other researchers have also used an inorganic copper(I) thiocyanate (CuSCN) hole transport layer (HTL) to enhance the power conversion efficiency (PCE) of Sb₂Se₃ cells by up to 7.5%. In various solar cells, the organic HTL 2, 2', 7, 7'-Tetrakis (N, N-di-p-methoxyphenylamine)-9, 9'-spirobi-fluorene (Spiro-OMeTAD) has been employed, including in Sb₂(S, Se)₃ cells with PCE values below 10% [19, 20]. However, large-scale production using organic HTLs is not advisable due to their unstable device performance and high cost. Therefore, it is crucial to develop a new, stable, cost-effective, and non-toxic material to produce efficient photovoltaic (PV) cells.

PEDOT: PSS is a popular choice as a hole transport layer (HTL) for perovskite solar cells (PSCs) due to its cost-effectiveness and ability to produce high-quality results. However, its highly doped nature can result in poor performance and stability compared to other HTLs, leading to issues such as interfacial recombination. To address this, researchers have explored additional p-doping of PEDOT: PSS to enhance its conductivity and match the energetics of the device, resulting in improved performance. For the electron transport layer (ETL), TiO₂ is commonly used and synthesized by annealing at temperatures above 450°C. However, to avoid high-temperature annealing, researchers have evaluated alternative metal oxides such as SnO₂ [21], In₂O₃ [4], WO₃, amorphous-TiOx [22], Zn₂SnO₄, and ZnO as potential ETLs for PSCs [23]. Among these, ZnO has shown promise due to its ultrahigh

electron mobility ($205\text{-}300\text{ cm}^2/\text{Vs}$), with recent research indicating that it can increase cell efficiency compared to TiO_2 [24]

In a PSC, the lower edge of the conduction band plays a crucial role in facilitating the transit of photogenerated electrons. Therefore, selecting an appropriate ETL with a suitable conduction band edge is crucial for achieving high performance in PSCs. Various researchers have used different techniques to enhance the ZnO semiconductor characteristics, and subsequently the PSCs' photovoltaic performance via doping and designing ZnO by employing other metal oxides or elements [28]. Even though these experiments were conducted, it was challenging for the researchers to enhance ZnO-based PSCs. ZnS was found to be similar with that of a ZnO wide bandgap semiconductor and it also showed comparable physical characteristics. With regards to quantum-dot-sensitised solar cells, ZnS showed outstanding electron mobility and was also seen to function like ETL and the interfacial passivation layer [28]. ZnS is associated with a low conduction band minimum (CBM) versus ZnO, making it a better match for MAPbI_3 -LUMO [25]. However, PSCs' photovoltaic performance still needs more improvement by employing ZnS or ZnO in order to facilitate the transportation of electrons to ZnO from MAPbI_3 [26].

In the past, a poor photovoltaic performance was displayed by the ZnS-based PSCs. The ZnO/ZnS nanoparticle structure can be employed to considerably decrease the optical band gap while simultaneously maintaining the required optical absorption value. As per the theory, the PSCs' open-circuit voltage (V_{oc}) follows the energy difference between the valence band maximum (VBM) and CBM (ELT) [27]. Thus, the V_{oc} value can be increased by adding ZnS to the ZnO-based PSCs [28]. Adding ZnS to the surfaces of ZnO behaves like an energy barrier that blocks the recombination of charges between MAPbI_3 and ZnO. However, this could also result in increasing ZnO-based PSCs' short-circuit current [29].

The simulation results showed that the carrier concentration in the absorber layer had a direct impact on the photovoltaic performance of the solar cell. An increase in carrier concentration led to an increase in the short-circuit current, which is a measure of the amount of current produced by the solar cell. Furthermore, the

simulation results also indicated that the band gap and energy level of the absorber layer played a crucial role in determining the photovoltaic performance of the solar cell. A wider band gap led to a lower short-circuit current, while a higher energy level of the absorber layer led to an increase in the open-circuit voltage, which is a measure of the voltage generated by the solar cell. The simulation results were also used to determine the optimal absorber thickness for the antimony trisulfide solar cell. The results showed that there was an optimal absorber thickness that maximized the photovoltaic performance of the solar cell. This optimal absorber thickness was dependent on the carrier concentration and the band gap of the absorber layer. In conclusion, this study demonstrates the importance of considering the link between carrier concentration, band gap, and energy level of the absorber layer on the photovoltaic performance of antimony trisulfide solar cells. The simulation results provide valuable insights into the design and optimization of these solar cells and could be used to guide future research and development in this field.

1.2 Problem Statement

Antimony selenide is a new emerging cell with higher absorption coefficient, low-cost nature, and earth abundant materials. Though higher efficiency is achieved in short period of time, they are not commercially available. This is due to the fact there are numerous factors limiting its use. The void formation at the back of interface and low open voltage due to carrier recombination loss caused by high intrinsic defects of the selenium. Additionally due to the material synthesis or deposition could achieve only 10.7% efficacy until now. This can be further designed with the use of suitable ETL, absorber layer and HTL to help increase efficiency of the cells.

1.3 The research questions

- I. What are the suitable parameters for the Antimony selenide absorber layer in solar cells?
- II. What are the suitable electron transport layer and hole transport layer for Antimony selenide solar cells?

- III. How does the planar structure of Antimony selenide solar cells affect their V_{oc} , FF, J_{sc} , and efficiency?

1.4 Research objectives

Three objectives have been designed to execute the research gap from the research areas mentioned in the problem statement. The objectives are as follows in this study:

- I. To select the suitable parameters for the Antimony selenide absorber layer
- II. To select suitable electron transport layer and Hole transport layer for Antimony selenide solar cells.
- III. To simulate the planar structure of the Antimony selenide solar cells to investigate V_{oc} , FF, J_{sc} , and efficiency by SCAPS-1D.

1.5 Research scope

The scope of this research study was to optimize the performance of Antimony triselenide solar cells by investigating various parameters using computer simulations. The main motive behind was to determine the optimal parameters for the absorber layer, including bandgap, thickness, carrier concentration, interface defect density, electron affinity, and energy level, using SCAPS-1D software simulations. Secondly to evaluate and select the most suitable Electron Transport Layer (ETL) and Hole Transport Material (HTM) for Antimony selenide solar cells. Finally, the third one was to conduct mathematical simulations of the solar cells with optimized parameters and materials, and to observe the resulting values of open-circuit voltage (V_{oc}), short-circuit current density (J_{sc}), fill factor (FF), and efficiency. With this the study aimed to contribute to the development of more efficient and reliable solar cells, with potential applications in renewable energy systems.

CHAPTER 2

LITERATURE REVIEW

2.1 Renewable energy

In recent decades, there has been a growing worldwide concern over global warming. The rising temperature of Earth's surface is primarily caused by human activities resulting in greenhouse a gas (GHG) emission which leads to depletion of the ozone layer. This was well deliberated in 2016 by global leaders, and the Paris Agreement goal was set to limit the rise in global temperature below 2°C [30]. Although growth in large scale agricultural food production and deforestation are implicated in causing global warming [31], production of energy by burning fossil fuels is one of the major sources of GHG emission. Due to rising demand in energy for purpose of heating, electrification, industrial operations and transport, there is need for production of energy from renewable sources which cause less GHG emission. The damage done by global warming to human life and natural ecosystems is evident everywhere. Global warming causes increased extreme weather conditions like heatwaves, storms, floods and disruption of food systems impacting physical and mental health of humans [32]. It is not just humans, but many animal and plant species have faced the dreaded consequences of this phenomenon and are forced to relocate to higher altitudes causing disruption in ecosystem.

Renewable energy comes from natural resources that can be replenished without consuming all the planet's resources in a human lifetime. These resources, includes biomass, tides, waves, sunshine, wind, rain, and thermal energy stored in the earth's crust that have the advantage of being accessible in some capacity almost everywhere. They also have the benefit of emitting little to no carbon dioxide, which makes them environmentally friendly. It has comparatively minimal expenses, which is advantageous for keeping energy rates at levels that are reasonable for everyone. Additionally, they are accessible to all, which is advantageous for growth and security as they are believed to be stable and endless [33]. On the other side, there is a limited supply of fossil fuels like oil, coal, and natural gas. They will eventually get exhausted as we keep extracting. Even if they are formed by natural processes, the

rate at which they are replenished is not as fast as the rate at which they are depleted by our consumption. Additionally, they have a number of drawbacks, which includes limited supply, a concentration of reserves in a few numbers of countries, and a significant contribution to pollution [34].

Although there has been good progress in development of technologies in harnessing renewable energy, still the world's energy needs are met from non-renewable energy sources. The latest Global status report, 2022 (GSR) as displayed in figure 1, showed that the total share of energy production was 78.5 % and 12.6% from fossils fuel and renewable energy respectively. The share of energy production from renewable energy increased from 8.7% in 2019 to 12.6 % 2022. As fossil fuels still are the major source of energy, its immense impact to climate change is a growing concern; therefore energy transition to low carbon emitting sources is imperative now. In addition to this, now in post covid era, and during the times of Russian Federation invasion of Ukraine, there is global issue in cost of fossil fuel due to problems in distribution, trade and transport of non-renewable energy [35].

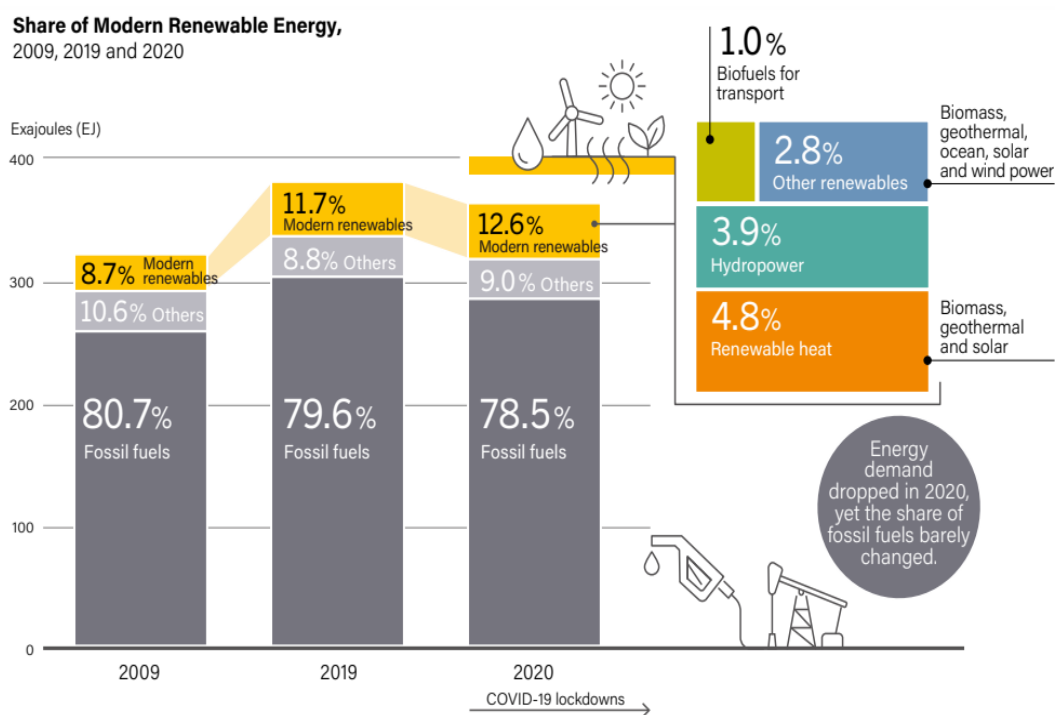


Figure 1 The share of the Modern Renewable Energy [35]

Nonetheless, owing to recent creative and less-expensive technologies for capturing and retaining wind and solar energy, renewables have grown in importance, accounting for more than one-eighth of total energy generation. Renewable energy is growing on a bigger scale, from solar panels on roofs to ground mounts that can sell power back to the grid to huge farms in the ocean. Even some whole rural towns use renewable energy to heat and light their homes[36]. The demand for renewable energy consumption continued to grow strongly, accounting for 40% of the global growth in energy level, showing an increase in energy with 3.2 EJ [37]

Among the various forms of renewable energy, solar energy has demonstrated exceptional efficacy in terms of energy output. According to an international energy agency (IEA) report from 2021, photovoltaic solar energy is still the most abundant renewable energy source, producing roughly 100 GW of energy per year. Additionally, as indicated in Figure 2, solar energy production has steadily increased over the past three years, going from 110 in 2019 to 150 in 2021.

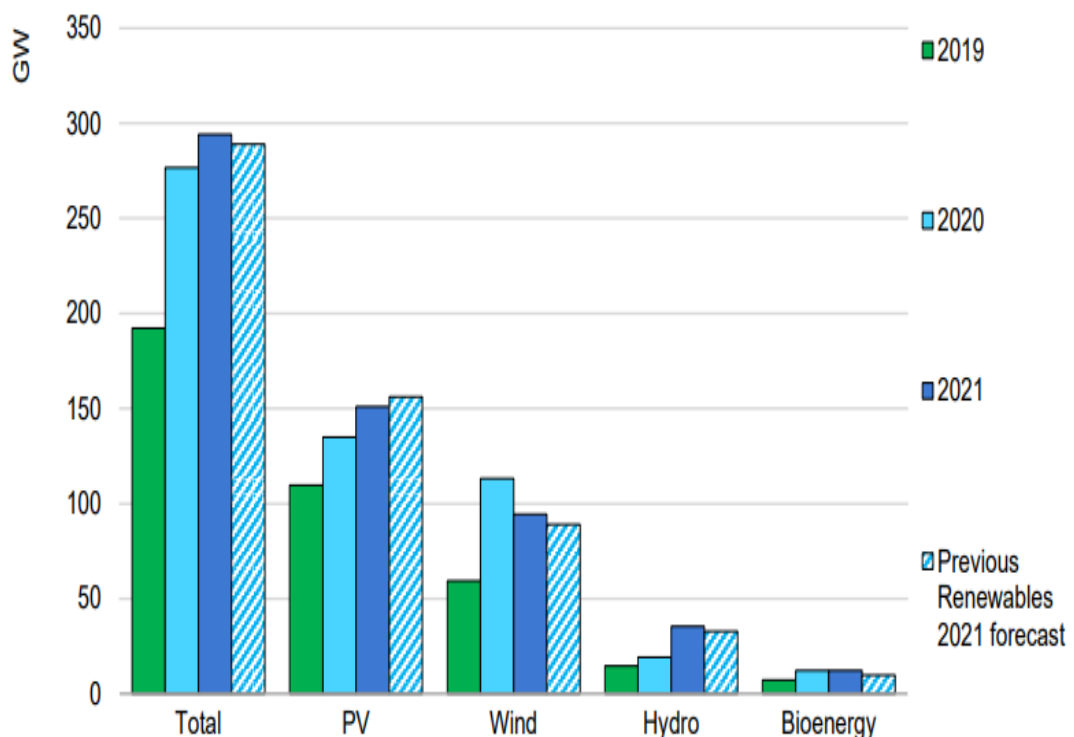


Figure 2 The net renewable energy production between 2019 and 2021 [38].

2.2 Solar PV Technology Installation

Energy generation from renewable resources has improved throughout time. These offer a more advanced, pure, and endless source of energy in the future. New, more energy-efficient technologies and larger, energy-producing installations are created every year. Figure 3 shows the overall amount of installed renewable power generation capacity increased by more than 200 GW in 2019, bringing the total to 2,588 GW by the end of the year. Installations dramatically increased from 2017, maintaining an average annual growth rate of more than 8% for the installed renewable power capacity over the previous five years. The addition of around 115 GW of solar PV on a global scale in 2019 solidified the technology's position as the leader in new energy producing capacity. 57% of the growth in renewable energy capacity last year came from solar PV (direct current), followed by wind power (60 GW) and hydropower (16 GW). Net additions of renewable energy generation capacity clearly outpaced net installs of nuclear and fossil fuel power capacity for the fifth year in a row.

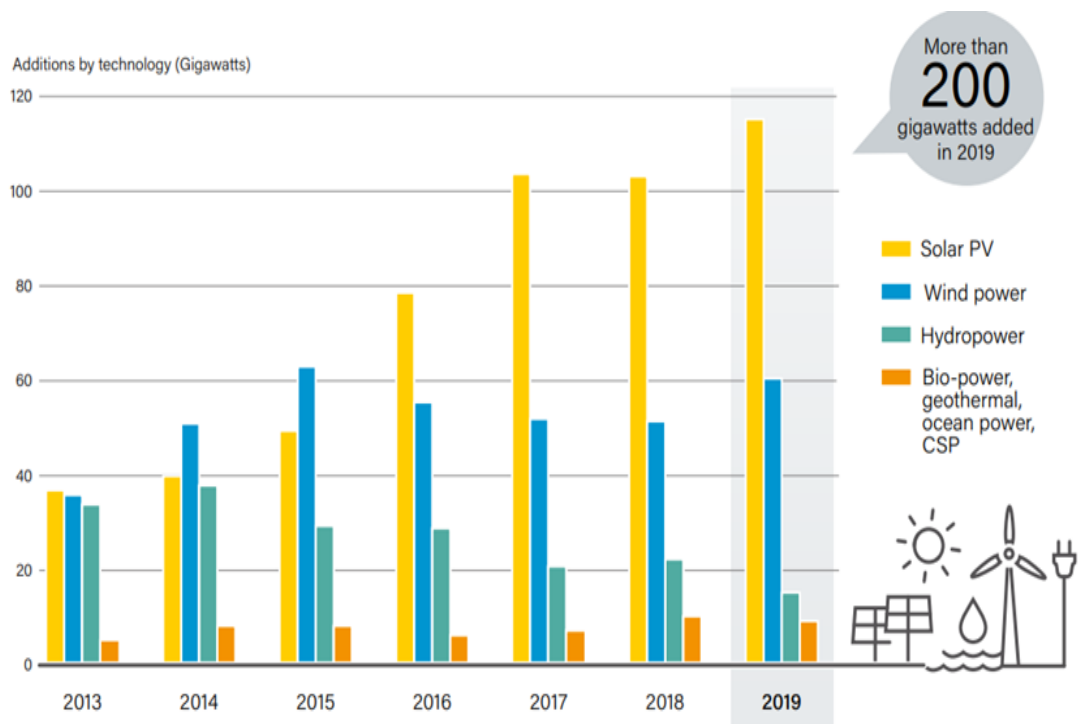


Figure 3 The overall amount of installed renewable power generation [35].

2.3 Solar energy

Energy is unquestionably a crucial part of socioeconomic growth that affects nearly every aspect of human life and a requirement for human development. Solar energy offers limitless energy from the sun, while some other energy sources such as hydro, wind, thermal, and oceanic energy all contribute to resolving the world's energy problems [39]. Solar energy was not a sudden invention; it dates to 200 years ago when the first solar cell was created. After that in 1839 Alexandre-Edmond Becquerel, a young French physicist, observed radiant energy being absorbed by material creating a current, while observing the photovoltaic effect. The availability of solar energy is one of the main factors influencing the economic feasibility of a solar system that can be converted into heat and electricity despite its installation cost, operation cost and lifetime of system components [40]. Solar energy offers a great deal of potential for producing reliable, safe, and clean energy. Because the sun has an infinite amount of energy, it can be used as an endless source of electricity for all time, whether directly or indirectly through the employment of concentrated solar power technology or photovoltaic cells. By converting the sun's energy into electric current, particularly through concentrated solar power, solar energy has demonstrated tremendous efficiency in the production of energy while its operations are efficient and functions effectively [41].

Solar cell

Solar cells are electrical device that accepts suns energy, use it, and helps to convert suns energy into electric energy by physical and chemical phenomenon. Solar cell is form of photoelectric device whose electric characteristic like voltage, current and resistance depends upon exposure to sun [42]. For high efficiency and to keep costs down, silicon is typically used to make solar cells. The design of solar cells has changed throughout several generations. The first generation of solar cells were made from silicon material that was single crystalline, polycrystalline, and amorphous. The highest efficacy for amorphous silicon obtained is 22.06% in 2021 [43, 44]. It is seen that single crystalline silicon solar cell has achieved 22.8% efficiency in heterojunction cells along with 15-17% efficiency by polycrystalline. However,

compared to polycrystalline cell amorphous have been seen more stable because it can withstand the shade and can absorb more radiation from the sun. Higher efficiency can be anticipated when employing single crystalline, although the price is higher than that of poly crystalline and amorphous materials [45]. Then, a more complex structure called a multi-hetero junction was introduced, emphasizing an improvement in efficiency and a drop in cost to make energy production more accessible to almost everyone. A ground-breaking technological innovation that uses organic materials to fabricate solar cells drastically reduces our dependence on semiconductors. Dye-sensitive solar cells (DSSC) are thin film solar cells which allow the user to turn both artificial and natural light into energy to power a variety of electrical devices. Despite having a lower efficiency, this method was projected to generate solar cells that were cheaper and simpler to make [46].

Solar cells are divided into three generations, the first of which contains solar cells that are comparatively expensive to manufacture yet have a high efficiency. The second-generation cells are with lower efficiency and cheap. The third generation is more effective with higher efficiencies and lower costs [47].

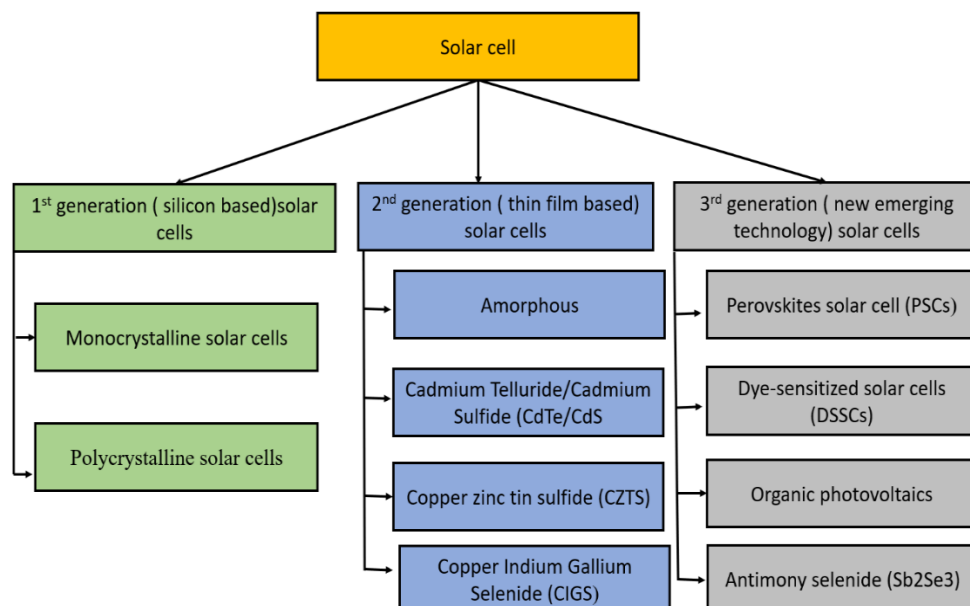


Figure 4 Classification of solar photovoltaic cells generation

First generation

First-generation solar cells had a high-power efficiency since they were built on silicon wafers, the oldest method [48]. Silicon wafers are the thin semiconductor slices used to produce chips for electronic devices. The types of first generation include Single Crystal (also called as monocrystalline silicon) and multi-Crystal Solar Cells (polycrystalline solar cells), which are the oldest and mostly used cells due to their efficiencies and cost effectiveness. Despite having few drawbacks, they are still widely used solar cells. Polycrystalline cells are constructed from silicon with several crystals, as opposed to monocrystalline cells, which are made from silicon with a single crystal. Monocrystalline silicon is prepared from pure silicon or doped silicon. Doped silicon is manufactured with only a small number of other elements to change its semiconducting properties [49]. Polycrystalline (also referred to as multi-crystalline or polysilicon) is produced using Siemens process from metallurgical grade silicon, where volatile silicon compounds are distilled and decomposed into silicon at high temperature. Multi crystalline ingots are manufactured and are further sliced into silicon wafers [50].

Second generation

The amorphous, Cadmium Telluride/Cadmium Sulfide (CdTe/CdS), Copper zinc tin sulfide (CZTS) and Copper Indium Gallium Selenide (CIGS) solar cells make up the second generation of solar cells, which are built on thin films. Amorphous silicon cells are created by depositing thin films on flexible substrates and are made from non-crystalline silicon. CdTe is combined with an n-type cadmium sulfide window layer, which has an optimal bandgap of 1.45 eV and a high absorption coefficient of $10^5/\text{cm}$, to generate a glass/transparent conducting oxide (TCO)/CdS/CdTe/Metal/Glass structure [51]. Amorphous cells are more expensive, require rigorous preparation conditions, and have significant environmental difficulties, but they are more resistant to shading and higher temperature than crystalline based cells. High photovoltaic conversion efficiency (PCE) of 15-20% was achieved in the lab using cadmium telluride and copper indium gallium selenium thin-film solar cells. However, due to the high cost of production and environmental risk posed by the lead content, industrial application is constrained [52]. CZTS is well

suitable for usage as a thin-film solar cell absorber layer because it has advantageous optical and electrical properties like CIGS (copper indium gallium selenide), but unlike CIGS (or other thin films like CdTe), CZTS is made up only of plentiful and non-toxic materials. Perovskite solar cells are known to be of greater interest due to their high conversion efficiency and cost effectiveness compared to silicon-based cells [25].

Third generation solar cells

Recently, third-generation solar cells have been developed to address the limitations of previous generations of solar cells. These include perovskites solar cells (PSCs), dye-sensitized solar cells (DSSCs), quantum dots solar cells, organic photovoltaics, and antimony selenide. These technologies are commercially less advanced but are emerging as superior with better stability, efficiency, and durability [53]. Perovskite solar cells (PSCs) are a promising third-generation technology due to their high-power conversion efficiency (PCE) and low production cost. PSCs have a theoretical efficiency limit of 31%, which is higher than that of silicon solar cells. However, the stability and durability of PSCs still need improvement, as they tend to degrade quickly under humid and hot conditions. Researchers are exploring new materials and device architectures to improve the stability of PSCs. Dye-sensitized solar cells (DSSCs) are another type of third-generation solar cell that uses a layer of dye-coated semiconductor particles to absorb light. DSSCs have a lower PCE than PSCs, but they have a longer lifespan and are more stable. DSSCs can also be made transparent, which makes them suitable for building-integrated photovoltaics (BIPV). However, the low PCE and relatively low stability still need to be addressed to improve their commercial viability.

Quantum dots solar cells (QDSCs) use semiconductor nanoparticles to absorb light and convert it into electrical energy. QDSCs have a high PCE and are easy to manufacture. They also have tunable bandgap, which makes them suitable for multi-junction solar cells. However, QDSCs suffer from stability issues and toxicity concerns due to the use of heavy metals in the production of quantum dots. Organic photovoltaics (OPVs) are a type of third-generation solar cell that uses organic

materials to absorb light and generate electrical energy. OPVs have low production cost, flexibility, and lightweight, which make them suitable for applications such as portable electronics. However, OPVs have a low PCE and suffer from low stability and durability. Antimony selenide (Sb_2Se_3) is a promising emerging solar cell material due to its high absorption coefficient, low toxicity, and earth-abundant elements. Sb_2Se_3 solar cells have achieved a PCE of up to 9%. However, the stability and reproducibility of Sb_2Se_3 solar cells still need to be improved. Though third-generation solar cells have the potential to overcome the limitations of previous generations of solar cells and pave the way for a sustainable and clean energy future. Researchers are exploring new materials and device architectures to improve the efficiency, stability, and durability of third-generation solar cells. However, more research is needed to overcome the challenges of commercialization and integration into the energy grid.

2.4 Perovskite Solar Cell

Perovskite is a mineral named after Lev Perovski and its structure inspired the development of perovskite solar cells. Perovskite Solar Cells (PSCs) are a type of thin-film photovoltaic cell with a unique crystallographic structure, making them more efficient in converting sun's photon energy into usable electricity[54]. The perovskite material is derived from calcium titanate (CaTiO_3) with a molecular structure of ABX_3 , where A is an organic cation such as cesium or methyl ammonium, B is a large inorganic cation like lead or tin, and X is a halogen anion like chloride or iodide as shown in the figure5. Organic-inorganic hybrid perovskites (OHIP) are a type of semiconductor material that exhibit unique optical and electrical properties compared to ordinary organic and inorganic semiconductors. Some of the advantages of OHIP materials include a large Bohr radius [55], weak binding energy, high dielectric constant [56], and high carrier diffusion velocity and length, making them ideal for fabricating highly efficient and cost-effective solar cells.

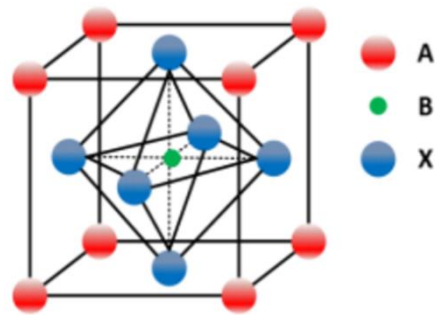


Figure 5: Molecular structure of Perovskite solar cell showing A, B and x [57]

Perovskite solar cells consist of an absorber layer, such as $\text{CH}_3\text{NH}_3\text{PbX}_3$, which is placed between an electron-transport layer (ETL) and a hole-transport layer (HTL) [58]. When the perovskite-absorber layer is exposed to light, it generates free charge carriers by inserting an electron and a hole into n-type and p-type carrier-transporting materials, respectively. The generated electrons travel through the mesoporous film and external circuit to reach the cathode, while the hole is diffused in the counter-electrode direction and recombines with the electron to provide current [59]. The thickness of the perovskite material determines the amount of current generated. Therefore, OHIP materials have become a prominent candidate for fabricating highly efficient solar cells due to their outstanding light-absorbing capacity and unique properties [60]. Displayed in Figure 6 is the overall composition of a perovskite solar cell, which encompasses several layers, such as the electrode, electron transport layer, absorber layer (perovskite), hole transport layer, and transparent conductive oxide layer.

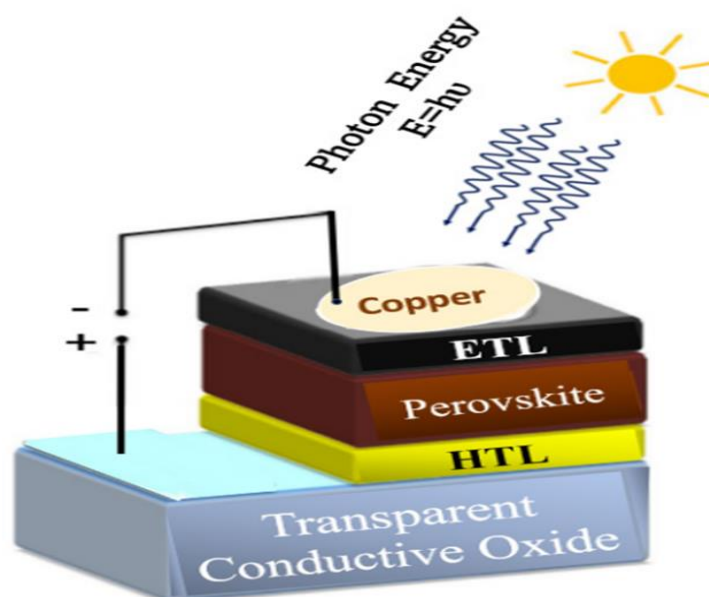


Figure 6: The device structure of a perovskite solar cell [61]

In 2009, Miyasaka and his team were the first to demonstrate the potential of perovskite materials in solar cell applications. They used $\text{CH}_3\text{NH}_3\text{PbX}_3$ as a sensitizer in dye-sensitized solar cells (DSSC), achieving a power conversion efficiency (PCE) of 3.81% [62]. Subsequent research has revealed that OHIP materials are highly promising candidates for solar cell applications due to the abundant availability of their precursor elements and the use of simple preparation techniques, such as vacuum-deposition and atmospheric solution-processing [63]. In a brief span of time, there has been a remarkable advancement in the field resulting in a significant improvement in the PCE, reaching an unprecedented high of 23.3% according to reference [64].

The use of efficient electron transport layer (ETL) is critical in the development of perovskite solar cells. Traditional perovskite solar cells utilize colloidal thin-film ETL made of SnO_2 [21], TiO_2 , ZnO or their mesoporous systems, which possess large grain boundaries and weak recombination at the interface. However, these semiconductor ETLs have inherent defects caused by oxygen vacancies and trap-assisted recombination. To address these issues, researchers have proposed various single-crystalline materials for use as ETL in perovskite solar cells. One promising material for ETL is the nano sheet or atom-thick transition metal dichalcogenides (TMDs) such as MoS_2 , WS_2 , and TiS_2 . These materials have a virtually defect-free thin structure that enables rapid transportation of charge carriers to the electrode. MoS_2 has low trap density and high carrier transportation ability, making it a popular choice for ETL. Additionally, due to its ambipolar property, it can also serve as a hole transport layer (HTL). In recent years, several studies have utilized MoS_2 as an ETL or HTL in perovskite solar cells. For instance, Kim et al.[65], fabricated a perovskite solar cell using MoS_2 as an HTL, achieving a power conversion efficiency (PCE) of 9.53%. Similarly, Das et al [66], used a MoS_2 thin film as an HTL in an inverted p-i-n heterojunction planar perovskite solar cell, achieving a PCE of 6.01%.

Malek et al.[67], demonstrated the preparation of atom thick MoS_2 nanosheets directly on indium tin oxide (ITO) substrate, which improved the homogeneity of the nanosheet at 200°C . The use of these prepared materials as ETL enhanced the

performance, stability, and interfacial charge transfer capability of the perovskite solar cell. As the size of the MoS₂ layer decreased, the PCE of the solar cell increased. Notably, a 5-atom-thick MoS₂ nanosheet ETL achieved a short-circuit current density (J_{sc}) of 16.24 mAcm⁻², an open-circuit voltage (V_{oc}) of 0.56 V, a fill factor (FF) of 0.37, and a PCE of 3.36%. Moreover, the MoS₂-based solar cell retained 90% of its initial PCE after continuous operation for 80 seconds under the irradiation of sunlight at maximum power point.

The hole-transporting layer (HTL) is crucial for improving the performance of photovoltaic devices. The efforts have been made to enhance its conductivity and suppress charge carrier recombination at the HTL and perovskite interface through doping. 2,2',7,7'-Terakis[N,N-di(4-methoxyphenyl)amino]-9,9'-spirobifluorene (spiro-OMeTAD) is a popular HTM due to its high solubility and glass transition temperature, but its insufficient oxidation states lead to poor PCE [68]. Kim et al. increased the oxidation time of spiro-OMeTAD using oxygen plasma, but this decomposes the perovskite phase to PbI₂, which can be resolved by doping with trivalent (p-dopants) materials[69]. Cobalt complexes and FeCl₃ can act as efficient p-type dopants, and acid additives can enhance the oxidation process and shorten the aging time of perovskite solar cells. Guan et al. investigated the effect of benzoic acid on the oxidation process of spiro-OMeTAD and found that it enhances the hole transportation capability of the HTL and reduces hysteresis in HTL-based perovskite solar cells, leading to an improved PCE of 16.26% under standard AM 1.5G illumination. Current research focuses on designing the HTL using acid additives and modifying the morphology of spiro-OMeTAD to further optimize its performance[68].

Perovskite solar cells have attractive properties such as strong optical absorption, high tolerance to defects, and the ability to tune their bandgap [70]. Despite the rapid development of perovskite cells, they are subject to long-term instability due to degradation from external factors such as water, light, temperature, humidity, and ultraviolet radiation. Another challenge is the toxicity of lead in perovskite cells, which can hinder their commercialization and advancement, and calls for the development of low-toxicity or non-toxic alternatives[71].

Antimony triselenide (Sb_2Se_3) is a semiconductor material that has been studied as a potential absorber layer in solar cells due to its suitable bandgap energy and high absorption coefficient, which makes it capable of efficiently absorbing a large portion of the solar spectrum. Additionally, Sb_2Se_3 is abundant and less toxic than some other semiconductor materials, making it a promising candidate for large-scale solar cell production. Perovskite solar cells, on the other hand, have recently gained attention due to their high-power conversion efficiency, ease of processing, and low cost. However, perovskite materials have some limitations, such as their instability and toxicity, which can limit their scalability and long-term stability. Therefore, the choice of absorber layer material in a solar cell depends on several factors, such as its bandgap energy, absorption coefficient, abundance, toxicity, stability, and cost. Sb_2Se_3 is a promising candidate due to its suitable properties and abundance, while perovskite materials have high efficiency but may have limitations in scalability and stability.

2.5 Antimony selenide (Sb_2Se_3)

Antimony selenide (Sb_2Se_3) is a type of semiconductor material made from less hazardous components, making it a promising candidate for use in solar cell absorbers[15]. It is part of a series of inorganic binary V2-VI3 compounds, which includes other materials like Bi_2S_3 , Bi_2Se_3 , Bi_2Te_3 , Sb_2S_3 , and Sb_2Te_3 [72]. These compounds, including Sb_2Se_3 , have an orthorhombic structure that naturally occurs in the mineral stibnite. The structure is formed by piling (Sb_4Se_6) n ribbons parallel to the [001] direction. The material is layered, and the layers are held together by van der Waals forces [73]. While the band gap of Sb_2Se_3 is higher (about 1.7 eV) than what is typically desired for single-junction solar cells, it is a good choice for multi-function tandem solar cells. In recent years, Sb_2Se_3 has gained significant interest due to its promising optoelectronic properties and environmentally friendly characteristics [74]. Despite the similarity in structure, only a few materials like Sb_2S_3 , Bi_2S_3 , and Sb_2Se_3 have been reported for use in photovoltaic (PV) applications[75].

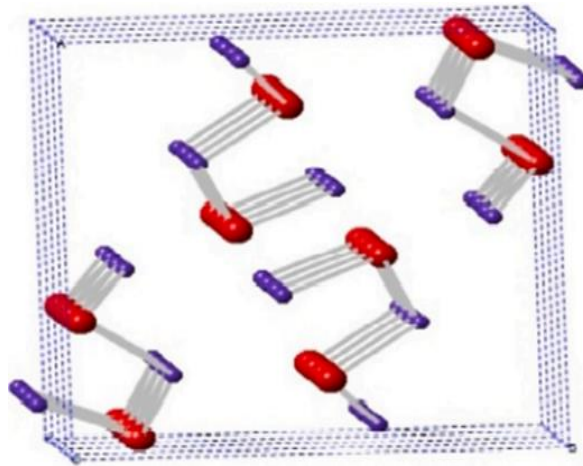


Figure 7 Crystal diagram of Antimony selenide [76]

Perovskite solar cells are a promising type of solar cell that use a perovskite material as the light-absorbing layer. Two elements, antimony (Sb) and selenium (Se), can be used in perovskite solar cells to improve their performance. Sb can be used as a dopant in the perovskite material to enhance its electronic properties. The introduction of Sb can increase the efficiency of charge transport within the solar cell, which results in a higher power conversion efficiency (PCE). Moreover, Sb can also function as a passivation agent to decrease the number of defects in the perovskite layer, which can further improve the solar cell's performance. Se can be utilized in perovskite solar cells as a substitute for sulfur (S). Se has a higher electronegativity than sulfur, which allows it to form stronger chemical bonds with other elements. This enhances the stability of the perovskite material, an essential factor for the solar cell's long-term performance. Additionally, Se can help to reduce defects in the perovskite layer, further improving the solar cell's overall efficiency. Moreover, the use of Sb and Se in perovskite solar cells can enhance their efficiency, stability, and performance. The electronic properties and energy levels of Sb and Se make them suitable for use in solar cells, and their introduction can contribute to efficient charge transfer and collection within the device. Furthermore, experimental studies have shown that incorporating Sb and Se into the perovskite structure can result in improved device performance. This is attributed to the fact that Sb and Se can modify the crystal structure of the perovskite, leading to improved stability, reduced defects,

and enhanced charge transport. Additionally, Sb and Se can help to reduce recombination losses, leading to higher open-circuit voltages and higher device efficiencies. Overall, the incorporation of Sb and Se into perovskite solar cells has the potential to significantly improve their performance and stability.

Sb_2Se_3 is a semiconductor with an orthorhombic crystal structure that is suitable for use in photovoltaic and thermoelectric devices due to its direct band gap of 1.1-1.3 eV[77]. The material is layered, and the layers are held together by van der Waals forces [73]. While the band gap of Sb_2Se_3 is higher (about 1.7 eV) than what is typically desired for single-junction solar cells, it is a good choice for multijunction tandem solar cells. In recent years, Sb_2Se_3 has gained significant interest due to its promising optoelectronic properties and environmentally friendly characteristics[74].

Antimony selenide is a promising material for various applications due to its high absorption coefficients, favorable electrical and magnetic properties, suitable band gap, low cost, and safety[78]. It has found applications in solar cells, photodetectors, batteries, and memory devices[79]. Antimony selenide is highly attractive for industrial production of low-cost thin-film solar cells due to its high absorption coefficient and excellent band gap, as well as its non-toxic and earth-abundant ingredients[80].

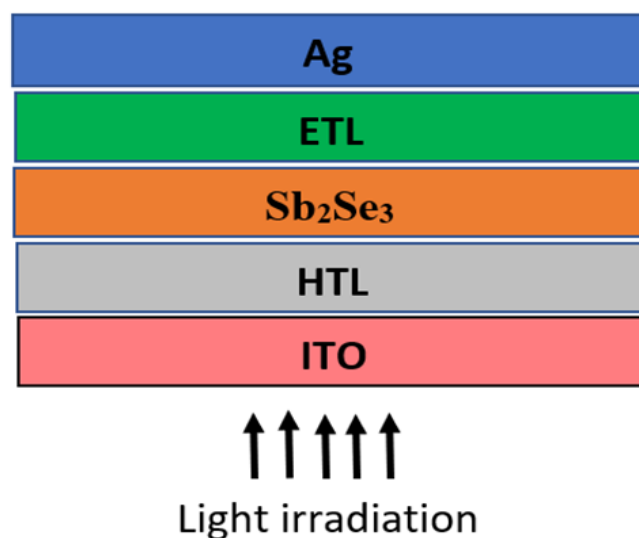


Figure 8 Schematic of the Sb_2Se_3 solar cell.

The absorption coefficient of a material refers to its ability to absorb light of a specific wavelength, with lower absorption coefficients indicating that light can penetrate deeper into the material [81]. The absorption coefficient is dependent on both the material and the wavelength of the light being absorbed. Semiconducting materials with higher absorption coefficients can more efficiently absorb photons, leading to the excitation of electrons into the conduction band. However, if the energy of the incoming photons is below the band gap, they will not be able to drive electrons into the conduction band, and the material will not absorb the light [82]. The absorption coefficient is not constant and varies greatly depending on the wavelength of the photons being absorbed. To efficiently produce electron-hole pairs, the absorber layer should have a high absorption coefficient ($>10^4 \text{ cm}^{-1}$) and an optimal bandgap of 1.1 to 1.3 eV. The choice of materials for designing solar cells is influenced by the absorption coefficients of different materials[83].

The refractive index of a material is defined as the ratio of the velocity of light in a vacuum to the velocity of light in the medium ($n=c/v$). For optimal optical properties, the refractive index of multiple layers in a solar cell should be roughly identical. By sandwiching a low refractive index layer between two high refractive index layers, a high density of states can be achieved, leading to greater interaction between the light and the material [84].

2.5.1 Antimony selenide structures

Recent years have seen advancements in the demonstration of Sb_2Se_3 solar cells with diverse device designs[85]. Mesoporous sensitized and planar architecture are the two basic categories for Sb_2Se_3 solar cell device topologies. Substrate and superstrate structures are two more divisions of the planar-type structure. In the production of Sb_2S_3 solar cells, both planar and mesoporous structures are utilized. Planar heterojunction could prevent high temperature annealing and minimize interface flaws when compared to the mesoporous construction[86].

The device is made up of different layers consisting of an electron transport layer (ETL) which converts photons into electrons and holes. A hole transport layer

(HTL) that has various roles as it extracts and transports holes in the active layer to the electrode. Secondly it acts as an energy barrier to prevent electron transfer to the anode. Thirdly it separates the absorber layer from the anode and isolates moisture in the air, improving device stability by reducing possible degradation and corrosion [87], and finally the electrode layers that connect the circuit externally to the conductive substrate [88]. Transparent electrodes are necessary for solar cells because they allow incoming light to reach the photoactive layer. Because of their transparency and conductivity, transparent conductive oxides (TCO) such as indium tin oxide (ITO) and fluorine doped tin oxide (FTO) are ideal for this application [89]. FTO (Fluorine-doped Tin Oxide) glass is a transparent conductive metal oxide that can be used to make transparent electrodes for thin film photovoltaics like amorphous silicon, Cadmium Telluride, Dye-sensitized solar cells and hybrid perovskites [36]. Other applications for FTO glass include touch screen displays, electromagnetic interference/radio frequency interference shielding, heated glass, anti-static coatings, and light-emitting diodes. FTO glass has several properties that make it suitable for the fabrication of a wide range of optoelectronic devices, including low surface resistivity, high optical transmittance, scratch and abrasion resistance, thermal stability up to its high temperatures and chemical inertness.

The following standard HTL was employed by the researcher in various solar cells: Tetrakis (N, N-di-p-methoxy phenyl-amine)-2, 2', 7, 7'-bis(9, 9-spirobifluorene) (Spiro-OMeTAD). Additionally, it was used in $Sb_2(S, Se)_3$ solar cells, which have a PCE value of 10% or below [53]. Nevertheless, because of their outrageous price and unpredictable device performance, using organic HTLs for large-scale production is not advised. Therefore, to produce functional photovoltaic (PV) cells, it is essential to develop a novel, stable, economical, and non-toxic material. PEDOT: PSS is the best option as an HTL for the creation of PSC because it is thought to be cost-effective and provides high-quality outcomes. PEDOT: PSS is widely and successfully used as an HTL for PSCs, however because of its highly doped nature; it performs poorly and is less stable than other HTLs. Numerous problems are the outcome, including acute interfacial recombination. To match the energetics and improve device performance,

the researchers changed and improved PEDOT: PSS conductivity by adding more p-doping.

In order to synthesize TiO_2 crystals, TiO_2 is used as an ETL and is typically annealed at temperatures higher than $450\text{ }^\circ\text{C}$. SnO_2 [21], In_2O_3 [4], WO_3 [90], amorphous- TiO_x [22], Zn_2SnO_4 [23], La-doped barium stannate (BaSnO_3) [20], and ZnO [91] were some of the metal oxides that were evaluated at low temperatures. Due to its high electron mobility ($205\text{--}300\text{ cm}^2/\text{Vs}$) among various ETLs, Zinc oxide (ZnO) was suggested as a suitable ETL [91]. According to Benami et al. (2022), using ZnO as an electron transport material improves cell efficiency as compared to TiO_2 [24].

Various researchers have used different techniques to enhance the ZnO semiconductor characteristics, and subsequently the PSCs' photovoltaic performance via doping and designing ZnO by employing other metal oxides or elements [25]. Though these experiments were conducted, it was challenging for the researchers to improve ZnO -based PSCs. ZnS was found to be similar with that of a ZnO wide bandgap semiconductor and it also showed comparable physical characteristics. With regards to quantum-dot-sensitized solar cells, ZnS showed outstanding electron mobility and was also seen to function like ETL and the interfacial passivation layer. ZnS is associated with a low conduction band minimum (CBM) versus ZnO , making it a better match for MAPbI_3 -LUMO [25]. However, PSCs' photovoltaic performance still needs more improvement by employing ZnS or ZnO in order to facilitate the transportation of electrons to ZnO from MAPbI_3 [26].

Previously, a poor photovoltaic performance was displayed by the ZnS -based PSCs. By using the ZnO/ZnS nanoparticle structure, the optical band gap can be significantly reduced while keeping the necessary optical absorption value. As per the theory, the PSCs' open-circuit voltage (V_{oc}) follows the energy difference between the valence band maximum (VBM) and CBM (ELT) [27]. Thus, the V_{oc} value can be increased by adding ZnS to the ZnO -based PSCs. Adding ZnS to the surfaces of zinc oxide behaves like an energy barrier that blocks the recombination of charges between MAPbI_3 and ZnO [28, 29]. However, this could also result in increasing

ZnO-based PSCs short-circuit current. This study concentrated on numerical simulation for demonstrating the link of carrier concentration, band gap, and energy level of the absorber layer on the antimony trisulfide solar cell's PCE. To consider different permutations about absorber thickness and identification of the quantum impact concerning solar cell parameters to increase simulation outcomes' applicability.

Shi et al. (2020) created Sb_2Se_3 thin film solar cells employing vacuum thermal evaporation and tris(8-hydroxy-quinolinato) aluminum (Alq_3) as an electron transport layer. As a hole transport layer, N, N'-bis(naphthalen-1-yl)-N, N'-bis(phenyl)benzidine (NPB) was used. The device architecture chosen was ITO/NPB/ Sb_2Se_3 / Alq_3 /Au. Power conversion efficiency (PCE) of 3.79%, a short circuit current density (J_{sc}) of 21.2 mA/cm^2 , and an open circuit voltage (V_{oc}) of 0.37 V were attained. The J_{sc} , V_{oc} , and PCE were significantly improved following the addition of an Alq_3 electron transport layer and reduction in charge recombination loss in the device [92]. Table (1) displays the literature-reported photovoltaic capabilities of HTL-free Sb_2S_3 solar cells along with absorber deposition techniques. To produce energy effectively, it is important to understand how different materials perform. The efficiency has altered as the year goes on due to changes in the materials used. Like this, the method of synthesis also has a significant impact on how particular materials perform.

| Device structure | Method | V_{oc} [V] | J_{sc} [mA cm^{-2}] | FF [%] | PCE [%] | Year/Ref. |
|---|------------------|--------------|----------------------------------|--------|---------|-----------|
| FTO/CdS/ Sb_2S_3 /Ag | T.E ^a | 0.6 | 6.12 | 35 | 1.27 | 2014/[93] |
| ITO/CdS/ Sb_2S_3 /Au | RTE ^b | 0.71 | 10.8 | 45 | 3.5 | 2016/[94] |
| ITO/CdSe/ Sb_2S_3 a)/Au | RTE ^b | 0.71 | 11.39 | 51.22 | 4.17 | 2017/[95] |
| FTO/CdS/ Sb_2S_3 /graphite | CSS ^c | 0.66 | 13 | 44.65 | 3.83 | 2018/[96] |
| FTO/c- TiO_2 /Cu-doped Sb_2S_3 /Au | RTE ^b | 0.64 | 15.16 | 47.64 | 4.61 | 2019/[97] |
| ITO/CdSe/ Sb_2S_3 /Au | VTD ^d | 0.71 | 15.7 | 43.2 | 4.73 | 2020/[98] |

- a. Thermal evaporation b. Rapid thermal evaporation c. Closed space sublimation. d. Vapor transport deposition

Table 1: Displays the literature-report of photovoltaic capabilities of HTL-free antimony trisulfide solar cells along with absorber deposition techniques.

The materials used in solar cells have been prepared and synthesized in a variety of ways. However, the efficiency has not been able to increase as much as it should for better sustainability up to this point. Likewise, the outcome displayed is varied with different efficacy when using different materials in different layers. As described in the literature, Table (2) below lists typical photovoltaic performances of Sb_2S_3 solar cells based on organic HTLs as well as absorber deposition methods. This clearly demonstrates how SCAPS can be used as a simulation device for materials at various levels to be further researched for improvement because the yield is greater than 30% when using antimony selenide as an absorber layer.

| Device structure | Method | Voc [V] | Jsc [mA cm^{-2}] | FF [%] | PCE [%] | Year/Ref. |
|--|------------------|---------|----------------------------|--------|---------|------------|
| TiO ₂ -c/Sb ₂ S ₃ /P3HT/PEDOT:PSS/Au | ALD ^a | 0.66 | 14.9 | 58 | 5.77 | 2014/[99] |
| SnO ₂ /TiO ₂ /Sb ₂ S ₃ /P ₃ HT/Au | CBD ^b | 0.58 | 10.57 | 2.80 | 45.24 | 2016/[100] |
| c-TiO ₂ /Sb ₂ S ₃ /Spiro-OMeTAD/Au | FCA ^c | 0.63 | 12.9 | 52 | 4.3 | 2017/[101] |
| c-TiO ₂ /Zn-dopeSb ₂ S ₃ /Spiro-OMeTAD/Au | Solution | 0.64 | 17.19 | 57.1 | 6.35 | 2018/[102] |
| c-TiO ₂ /C60-modified Sb ₂ S ₃ /Spiro-OMeTAD/Au | Spin coating | 0.49 | 8.44 | 42.15 | 1.75 | 2019/[103] |
| c-TiO ₂ /m-TiO ₂ /Co-doped Sb ₂ S ₃ /P3HT/Ag | Spin coating | 0.42 | 6.84 | 46 | 1.33 | 2019/[104] |

| | | | | | | |
|---|--------------|-----|----|----|----|------------------------|
| TCO/ZnS/Sb ₂ Se ₃ /PEDO T: PSS | SCAPS 1-D | 1.0 | 34 | 85 | 30 | 2022/This work [44] |
|---|--------------|-----|----|----|----|------------------------|

a. atomic layer deposition b. chemical bath deposition c. facile chemical method

Table 2 Displays the performances of Sb₂Se₃ solar cells based on organic HTLs, as well as absorber deposition techniques.

Mesoporous sensitized structure

A mesoporous sensitized structure (MSS) is a type of solar cell that utilizes a mesoporous oxide semiconductor film sensitized with a dye molecule to enhance its light absorption properties[105]. This structure consists of many small pores, typically with diameters ranging from 2-50 nm, providing a large surface area for dye absorption and electron transfer. The sensitization process involves immersing the mesoporous oxide film in a solution containing a dye molecule, which then adsorbs onto the surface of the oxide particles. When the dye molecule absorbs light, it generates an excited state electron, which is injected into the conduction band of the oxide semiconductor, leading to the generation of an electrical current. To construct an MSS-based solar cell, a mesoporous scaffold layer made of a wide bandgap metallic oxide, typically TiO₂, is deposited onto a conductive substrate such as indium tin oxide or fluorine-doped tin oxide[106]. An absorber layer made of a material such as Sb₂Se₃ is then added on top, followed by a hole transport layer (HTL) and a metal electrode such as Au. The mesoporous scaffold structure compensates for the short minority carrier diffusion length in the absorber layer, which would otherwise slow down electron transport[107]. Researchers are currently working on developing mesoporous sensitized-type Sb₂Se₃ cells, which have evolved from solid-state dye-sensitized solar cells (DSSCs). However, despite ongoing research, mesoporous cell efficiencies remain below 3% due to charge carrier recombination at the mesoporous TiO₂/ Sb₂Se₃ interface. Figure (9) below shows the mesoporous structure of Sb₂Se₃ [108].

Planar Structure

Antimony selenide (Sb_2Se_3) has a layered crystal structure, with each layer consisting of covalently bonded SbSe_3 pyramids linked through Se atoms. The layers are held together by weak van der Waals forces, allowing for easy cleavage and exfoliation of the material [107]. Each Sb_2Se_3 pyramid in the crystal structure is a trigonal pyramid with three Se atoms at the base and one Sb atom at the apex. The Se atoms are arranged in a triangular plane, while the Sb atom sits above the center of the plane. The layers of Sb_2Se_3 are stacked in an ABAB... sequence, where adjacent layers are shifted by approximately half the unit cell length in the c direction. This results in a rhombohedral crystal lattice with a space group of $R\bar{3}m$. The planar structure of Sb_2Se_3 and its layered nature make it a promising material for electronic and optoelectronic applications, such as solar cells and thermoelectric devices [109].

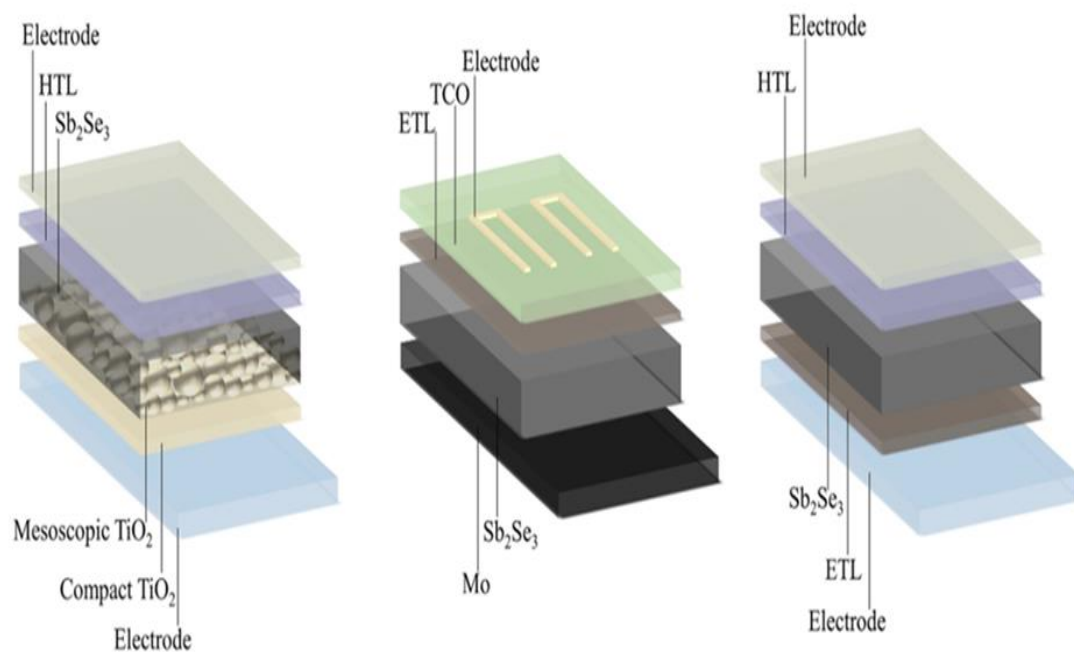


Figure 9 Schematic representations of three common Sb_2Se_3 solar cell devices Architectures: (a) mesoporous sensitized structure; (b) Substrate planar structure; and (c) Superstrate planar structure [106].

The substrate structure consists of several components including a glass substrate coated with molybdenum-disulfide, an absorber layer made of antimony selenide, an ETL layer (such as cadmium sulfide), a transparent conductive oxide

(TCO) layer made of materials like zinc oxide or indium tin oxide (ITO), and a grid electrode (usually made of silver). Among TCO materials, ITO is preferred due to its superior optical and electrical properties. However, the cost and manufacturing process of ITO are not ideal as indium, its primary raw material, has certain drawbacks. There are no strict requirements for substrate materials if they do not negatively affect the cell's performance. This substrate structure is illustrated in Figure 9 (b)[110].

Superstrate planar structure

The superstrate device configuration primarily consists of a TCO substrate, an ETL layer, an Sb_2Se_3 absorber layer, an HTL layer, and a metal electrode (Figure 9c). Recent studies have shown the existence of two device architectures in superstrate configurations: p-i-n and n-i-p. Here, p, I, and n refer to acceptor-type semiconductors, intrinsic-type semiconductors, and donor-type semiconductors, respectively. To enhance carrier extraction efficiency, the quasi-intrinsic absorber is typically accompanied by p-type high-temperature leak layers (HTLs) and n-type electron transport layer (ETLs). Building a n-i-p device configuration can also create a back surface electric field, which limits carrier recombination at the back surface[111]. To reduce the amount of back surface electric field, it is necessary to reduce carrier recombination.

However, the practical application of the superstrate device configuration is limited by the requirement that the substrate material be transparent in the viewable region. Compared to the superstrate-type Sb_2Se_3 solar cells with champion cell efficiency of 7.6%[112], the substrate-type Sb_2Se_3 solar cells have higher efficiency at 9.2%[21]. The planar superstrate Sb_2S_3 structure device has been claimed to have the best efficiency to date, which is 7.10% [113]. Figures 10 shows the year-by-year PCE progress of Sb_2S_3 -planar and Sb_2S_3 -sensitized structural devices [114]

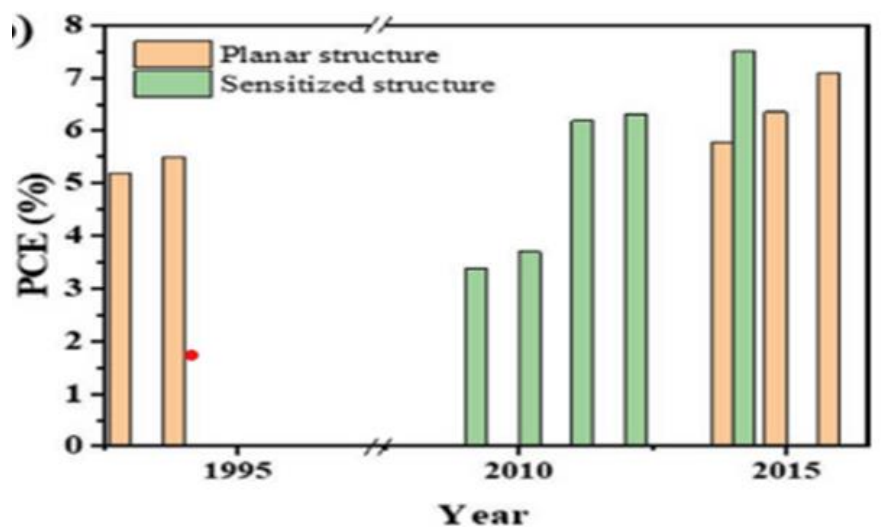


Figure 10 Displays sensitized solar cells and planar solar cells [114]

2.5.2 Present Status of Antimony selenide Solar Cells

Antimony selenide is a semiconductor material that has a high absorption coefficient for sunlight, which makes it a good candidate for use in solar cells. These compounds are composed of antimony (Sb) and chalcogenide elements (sulfur, selenium, or tellurium). They are being studied as potential light-absorbing materials for thin-film solar cells because they are earth-abundant, environmentally benign, and have long-term stability. Among the antimony chalcogenides, Sb_2S_3 has received the most attention as a solar cell absorber material due to its excellent optoelectronic properties. However, Sb_2Se_3 and mixed chalcogenide $\text{Sb}_2(\text{S},\text{Se})_3$ also show promising results as absorber materials, with Sb_2Se_3 having a higher absorption coefficient than Sb_2S_3 and $\text{Sb}_2(\text{S},\text{Se})_3$ having tunable bandgaps [115].

The efficiency Figure (11) shows how antimony chalcogenide solar cells have advanced significantly. Sb_2X_3 solar cells have been the subject of ongoing study since 2009. Due to its effective band gap with 1.7 eV Using a structure of $\text{P}_{25}/\text{In-OH-S}/\text{Sb}_2\text{S}_3/\text{KSCN treatment}/\text{CuSCN}/\text{Au}$, the Hodes group initially used Sb_2S_3 as a sensitizer in 2009 to create sensitized solar cells, which showed an initial PCE of 3.37% [114]. Seok group came next in 2009, 5.13% was raised by purposefully including poly (3-hexylthiophene) (P_3HT) as a hole conductor in Sb_2S_3 solar cells.

Interfacial recombination was successfully controlled due to the favorable energy band matching and strong hole mobility of the P₃HT layer [116]. The same group created a series of HTMs in 2011 that increased the PCE of Sb₂S₃ sensitized solar cells above 6%, including PCPDTBT, PTAA, PCDTBT, and P₃HT[117].

In 2014, the Seok group achieved an efficiency of 3.21% for the first Sb₂Se₃-sensitized structure using a spin coating process[118]. However, initially, the reported efficiency was less than 1%, with Sb₂Se₃ having a band gap 1.1 eV narrower than Sb₂S₃[119]. Subsequently, the development of planar-type Sb₂Se₃ solar cells with a PCE of 2.26% was a significant breakthrough, attracting widespread interest in Sb₂Se₃[13]. Since then, the Tang Group has set a series of records, including 3.7% in 2014[120], 5.6% in 2015[121], and 6.5% in 2017[18], using the rapid thermal evaporation (RTE) approach. RTE is a process like close space sublimation, where the vapor is confined to a small area and quickly settles on the substrate. The same group further improved the efficiency of Sb₂Se₃ solar cells to 7.6% in 2018 using vapor transport deposition (VTD) [112].

In 2018, the Tang group used the rapid thermal evaporation (RTE) method to create the Sb₂S₃ absorber layer and then fabricated Sb₂S₃ solar cells with a power conversion efficiency (PCE) of 3.5% [94]. Later that year, the Chen group incorporated Zn²⁺ into Sb₂S₃ using n-type doping and achieved a record PCE of 6.35%. More recently, in 2020, the Li group modified the TiO₂ electron transport layer using zinc halides such as ZnCl₂, ZnBr₂, and ZnI₂. This modification improved the electrical properties of the layer and passivated any defects. As a result, the group was able to manufacture Sb₂S₃ solar cells with a PCE of 7.08% [94].

In 2019, Mai and colleagues used the closed space sublimation (CSS) approach to deposit arrays of [001]-oriented Sb₂Se₃ nanorods on Mo-coated glass substrates. They produced non-planar heterojunction core-shell solar cells that demonstrated a verified 9.2% efficiency, the highest known PCE for Sb₂Se₃ solar cells with substrate structure. These advancements in Sb₂Se₃ solar cell technology demonstrate the potential for further improvements in efficiency and performance in the future[21].

In 2019, Dang et al. were able to achieve 6.14% efficiency in creating the $\text{Sb}_2(\text{S},\text{Se})_3$ absorber by utilizing an in situ hydrothermal and post-selenization approach[4]. The Cheng Group made a significant advancement in 2020 by achieving a record efficiency of 10.0% using a low-temperature hydrothermal deposition method that resulted in high-quality $\text{Sb}_2(\text{S},\text{Se})_3$ films with a preferred ribbon orientation[122]. Subsequently, the group added ethylenediaminetetraacetic acid (EDTA) to the hydrothermal reaction precursor, which improved the electrical characteristics of the films and enabled the regulated deposition process, leading to an increase in the power conversion efficiency (PCE) of $\text{Sb}_2(\text{S},\text{Se})_3$ solar cells to 10.5%[123]. Our project further optimized different parameters using SCAPS 1-D device and projected an efficiency of 30%. Figure 12 illustrates the significant progress in the efficiency of $\text{Sb}_2(\text{S},\text{Se})_3$ solar cells, which has increased from 0.13% in 2009 to 9.2% in 2018[124].

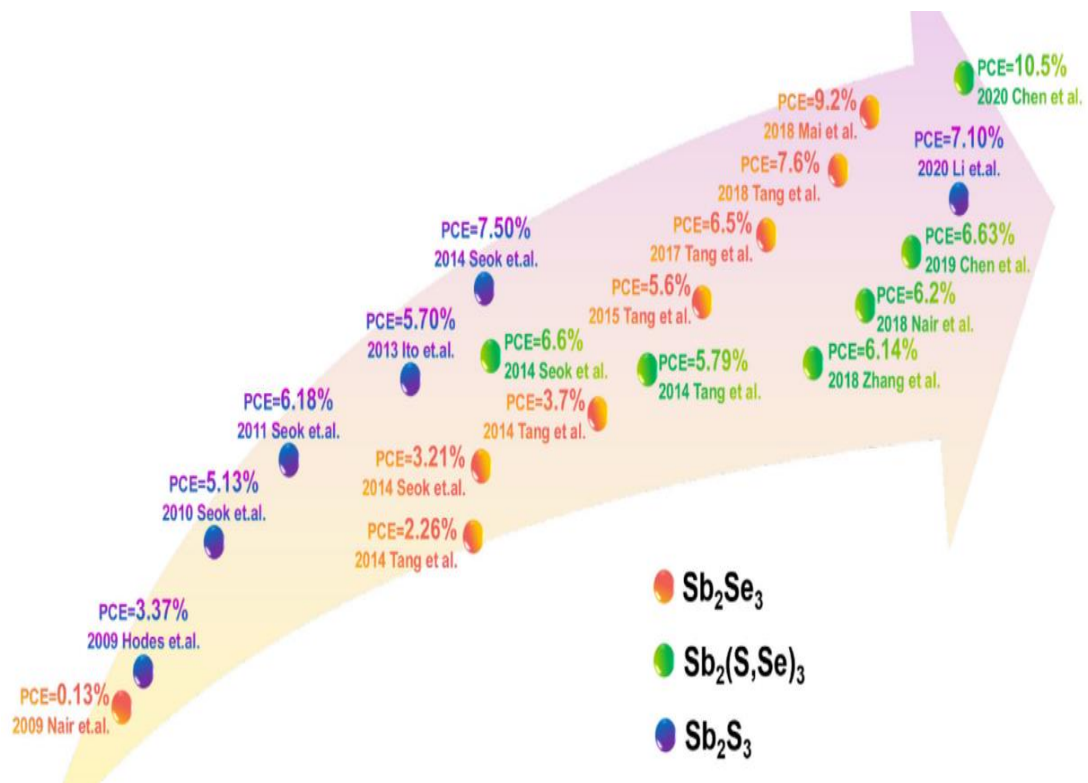


Figure 11 The significant developments in antimony chalcogenide solar cells [124]

2.6 Solar cells simulators and current-voltage measurement

The evaluation of solar energy considers various parameters that affect solar radiation, including the solar spectrum's different wavelengths of photon energy, which can be lost as the energy interacts with different substances in the atmosphere on its way to the earth's surface[125]. Additionally, solar radiation is influenced by factors such as sun zenith angles, changes in height, and moisture content in the air, all of which can cause fluctuations in the amount of solar energy received. To measure the air thickness, the industry standard is to use the Air Mass (AM) 1.5 spectra, which considers weather conditions throughout the year as chosen by the American Society for Testing and Materials (ASTM)[126]. This metric represents the length of the path taken by light through the atmosphere and is normalized to the shortest possible length. Moreover, the incident power density from the sun is a rounded value of 1000 W/m². The solar zenith angle, which is the angle between the sun and the zenith, is 48.2°[127].

Solar cells are semiconductor devices that directly convert solar energy into electricity, making them highly efficient and sustainable sources of energy. The performance of the materials used in solar cells is greatly influenced by various parameters, which can be adjusted and varied to determine their workability [128]. However, to produce a better and more sustainable energy source in the long run, it is crucial to consider the efficiency of the energy source. In the simulation of materials using SCAPS 1-D, important parameters include thickness, bandgap, electron affinity, conduction and valence band effective density of states, electron, and hole thermal velocity. The thickness of the material is particularly important in determining the amount of light that can be captured. Therefore, it is essential to maintain the optimal thickness of materials like Sb₂S₃ as too thin a layer may reduce the open-circuit voltage (VOC) and short-circuit current density (JSC), leading to severe shunt and insufficient absorption [129].

Band gap

In a solar cell, the bandgap refers to the energy difference between the valence band and the conduction band of the semiconductor material used in the cell as

illustrated in figure 7[130]. When photons (particles of light) hit the solar cell, they are absorbed by the semiconductor material, causing electrons in the valence band to become excited and jump to the conduction band. This creates an electron-hole pair, where the electron is in the conduction band and the hole (a vacancy where an electron used to be) is in the valence band [131]. The electrons in the conduction band can then move freely through the material and be collected as electrical current, while the holes in the valence band can move in the opposite direction.

However, for this to happen efficiently, the bandgap of the material must match the energy of the incoming photons. If the energy of the photons is too low (i.e., their wavelength is too long), they will not have enough energy to create an electron-hole pair and will pass through the material without being absorbed. Conversely, if the energy of the photons is too high (i.e., their wavelength is too short), they will create electron-hole pairs with excess energy that will be lost as heat, reducing the overall efficiency of the solar cell [132]. Therefore, choosing a semiconductor material with an appropriate bandgap is crucial for designing an efficient solar cell. Short-circuit current is reduced when the band gap is bigger than 1.21 eV because the layer's absorption is reduced. The open circuit voltage, on the other hand, rises linearly with the band gap fluctuation. When the short circuit current declines with the increasing bandgap, the open circuit voltage also increases as the band gap increases. Since in an ideal device the V_{oc} is limited by the radiative recombination [133].

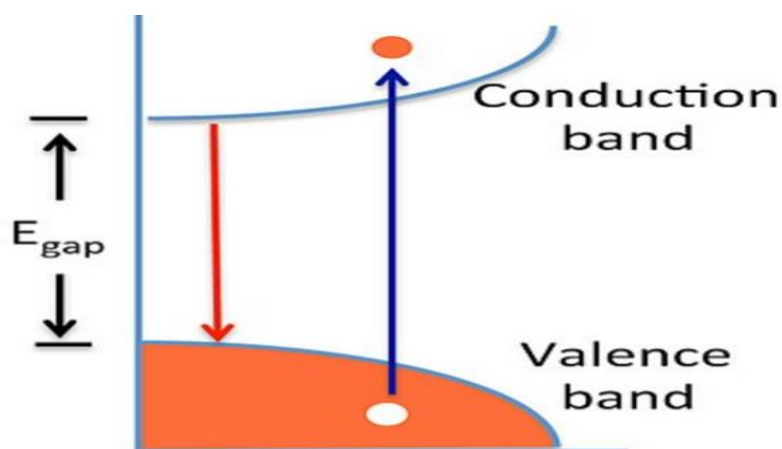


Figure 12 The density of states [130].

The main parameters involved in IV characterization are mentioned below.

- Short-circuit current (I_{sc}),
- Open-circuit voltage (V_{oc}),
- Maximum power point (P_{max}),
- Maximum cell current (I_{max}),
- Maximum cell voltage (V_{max}), and
- Fill factor (FF)

Short circuit current (I_{sc})

In a solar cell I_{sc} is the maximum current that can be generated by the cell when there is no external load connected to it, and the external circuit is shorted [134]. A short circuit exists whenever the resistance of a circuit or the resistance of a part of a circuit drops in value to almost zero ohms. A short often occurs because of improper wiring or broken insulation [135]. It is measured in amperes (A) or milli-amperes (mA). Short circuit values vary depending on factors like cell area, solar energy that hits the cell and cell design [136]. "J" stands for current density, and " J_{sc} " stands for short circuit current density. By dividing the short circuit current by the area of the solar cells, the short circuit current density is calculated by the formula $J_{sc} = I_{sc} / A$ [137].

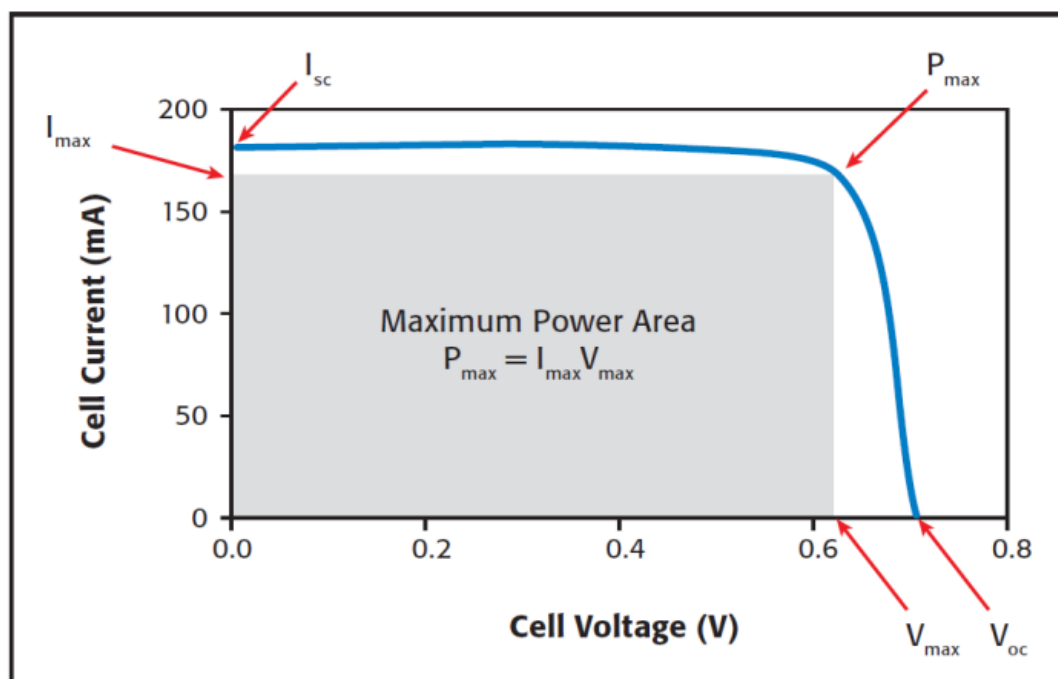


Figure 13 The current-voltage characteristics of a solar cell [139]

When the external circuit is shorted, the current flows freely through the cell, and the I_{sc} is limited only by the solar cell's ability to generate current. The I_{sc} is a fundamental parameter that characterizes the performance of a solar cell, as it represents the maximum current that the cell can generate under standard test conditions (STC), which include an irradiance of 1000 W/m^2 , a cell temperature of 25°C , and an air mass of 1.5 [138]. The I_{sc} is an important parameter because it provides a baseline for determining the maximum power that the solar cell can deliver, and it is used in combination with other parameters, such as the open circuit voltage (V_{oc}) and the fill factor (FF), to predict the performance of the solar cell under different operating conditions [136].

Maximum Power Point (P_{max})

It is the greatest amount of usable electrical power that can be generated by a single solar cell when tested under ordinary conditions [143]. The current at which maximum power is produced is known as the current at maximum power point. The voltage at which maximum power is produced is known as the voltage at maximum power point. The I-V characteristics of a solar cell are given by V_m and include the voltage at the Maximum Power Point (V_{max}) [127].

Open circuit voltage (V_{oc})

Open circuit is determined by determining the voltage that is present between the terminals of the cell when there is no load attached to the cell. This voltage is dependent on the procedures used in manufacturing as well as the temperature; however, it is not proportional to the amount of light or the surface area that is exposed. The voltage of a solar cell in open circuit is close to being equivalent to 0.5 to 0.6 volts. Typically, it is indicated by the symbol V_{oc} [140].

Closed circuit voltage.

The closed-circuit voltage in a solar cell refers to the voltage that is generated when the solar cell is connected in a closed circuit with a load, such as a battery or an electrical appliance [141]. It is the maximum voltage that the solar cell can produce

under a specific set of operating conditions. The closed-circuit voltage of a solar cell depends on various factors, such as the materials used to make the cell, the amount of sunlight hitting the cell, the temperature of the cell, and the load resistance. Generally, the closed-circuit voltage increases with increasing levels of light intensity and decreases with increasing temperature[142].

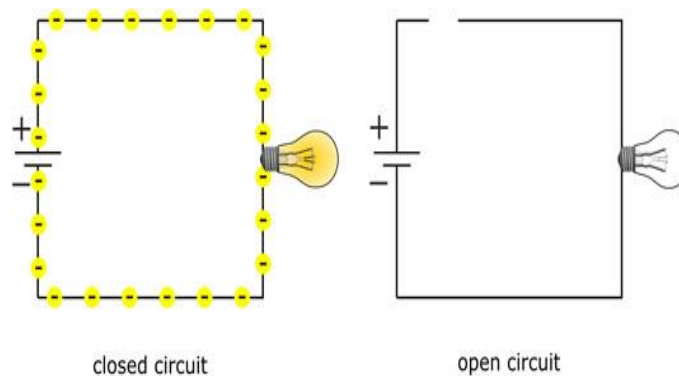


Figure 14: The illustration of closed and open circuit

Fill factor (FF)

Fill factor represents the ratio of the solar cell's short circuit current and open circuit voltage to its product of current and voltage at its peak power point [144]. The FF value goes down because of series resistance and shunt resistance. Leakage of current through the cell due to local defects at the junction or shunts at the edges of solar cells causes shunt resistance [145]. When the photo-generated carriers reach the external circuit, series resistance forms from the total of the resistances along the current route. The fill factor is reduced most significantly by series resistance.

$$\text{Fill Factor} = (V_{oc} \times I_{sc}) / (V_{max} \times I_{max})$$

The power conversion efficiency: Output power (P_{max}) / (Input power) [1]

A photovoltaic (PV) cell circuit is made up of several components, including:

Light-induced current source (IL)

This is the current produced by the PV cell in response to incoming light. Series resistance (r_s): This resistance is added to the circuit to reduce the short circuit current and increase the power output. Shunt resistance (r_{sh}): The shunt resistance represents the energy loss due to surface leakage along with the cell's edge or crystal defects. Ideally, r_s and r_{sh} should be zero ohms ($r_s = 0$) and infinite ($r_{sh} = \infty$) to achieve the highest efficiency. However, in practice, there will always be some resistance present [57].

Load resistor (RL)

A load resistor in a solar cell system refers to an external component that is connected to the output terminals of the solar panel or module to convert the electrical energy produced by the solar cells into a usable form. Its value is determined by the application and desired performance. By optimizing the values of these components and minimizing their losses, the efficiency and performance of the PV cell can be improved [146]. The load resistor in a solar cell system converts the DC energy produced by the solar cells into usable power. The right value of load resistor is crucial for optimizing power output. If the load resistance is too low, the solar cell may be damaged, while if it's too high, power output will be limited.

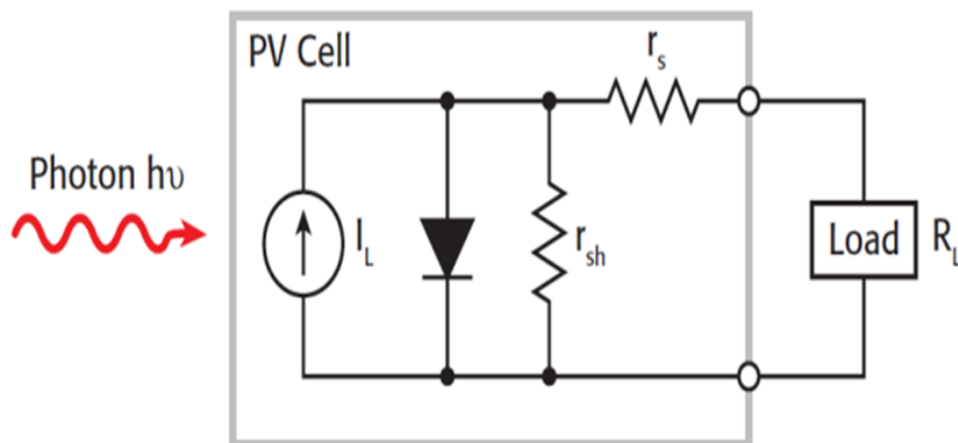


Figure 15: circuit diagram of a PV cell [57]

Quantum efficiency

The ability of a solar cell to convert incident photons into electrical current. It is a measure of the ratio of the number of electrons generated by the solar cell to the number of incident photons. Quantum efficiency is typically measured as a function of the photon wavelength or energy and can provide valuable information about the performance and efficiency of a solar cell across the solar spectrum. A higher quantum efficiency at a given wavelength means that the solar cell can more effectively convert photons of that energy into electrical current and is therefore more efficient overall.

Efficiency Value

Efficiency value represents the ratio of the power output of the cell to the power input from the sun. The efficiency value of a solar cell is determined by several factors, including the type of material used, the design of the cell, and the manufacturing process[147]. The theoretical maximum efficiency of a solar cell is known as the Shockley-Queisser limit, which is around 33% for a single-junction cell. However, in practice, most commercial solar cells have efficiencies ranging from 15% to 25%. This means that only a fraction of the sunlight that hits the cell is converted into usable energy, and the rest is either reflected or converted into heat. Efficiency is a key factor in selecting solar cells for a specific application. Higher efficiency cells generate more power per unit area and require fewer cells to achieve a certain power output.[148].

To improve the efficiency of solar cells, two methods are used. The first involves selecting suitable semiconductor materials that match the solar spectrum[149], while the second method involves innovative device engineering. Solar cell efficiency is represented by the symbol η and is calculated by dividing the maximum electric output power generated by the total power of the incident light P_{in} [150] .

$$\eta = \frac{V_{mmp} \cdot I_{mmp}}{P_{in}} = \frac{V_{oc} I_{sc} FF}{P_{in}}$$

CHAPTER 3

RESEARCH METHODOLOGY

3.1 Materials

3.1.1. Simulation parameters

The researchers used the SCAPS-1D tool, a 1-D solar cell device simulator developed at the University of Gent [25] to model and simulate a Sb_2Se_3 absorber-based thin film solar cell. The semiconductor device was constructed by implementing the Poisson's, drift-diffusion, and carrier continuity equations through SCAPS-1D simulation [151]. The researchers used the SCAPS-1D simulator to study the many characteristics of PV devices, including their recombination profiles, current-voltage (I-V), capacitance-voltage (C-V), and capacitance-frequency (C-f). The findings demonstrated that a few variables, including doping concentration, electron affinity, interface defect density, cell thickness, operating temperature, bulk defect density, resistances, and quantum efficiency metal work function, have an impact on the device's performance. All simulations were carried out under the same lighting conditions of 100 mWcm^2 , 300 K temperature, and AM1.5 G light spectrum. Figure 16 depicts the structure of the $\text{ZnS}/\text{Sb}_2\text{Se}_3/\text{PEDOT: PSS}$ heterojunction device.

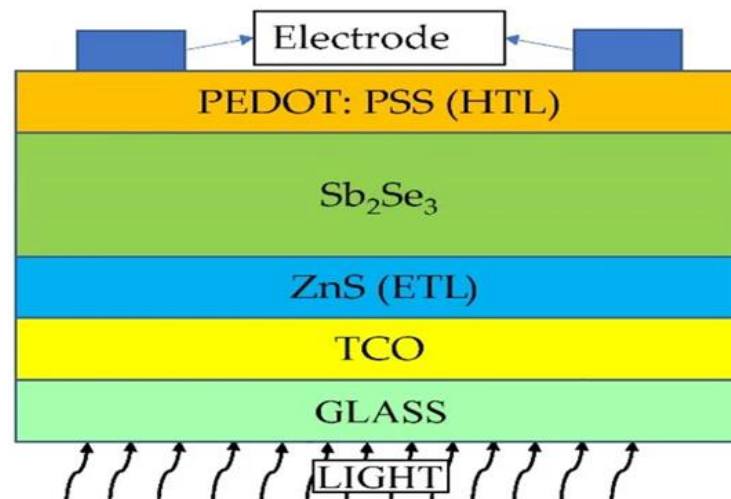


Figure 16 Structure of the Sb_2Se_3 solar cell device

According to the structure, the p-type Sb_2Se_3 absorber as well as the rear metal contact was coupled by an ultrathin p-type PEDOT: PSS as HTL. In the device,

fluorine-doped tin oxide (F: SnO₂) and the n-type ZnS were included in the TCO layer and ETL. Moreover, in the TFSCs, aluminium (Al) was employed to construct the front and rear metal contacts [152]. Table 3 shows how the physical parameters are considered in the simulation. The values of material parameters employed in the numerical computation are taken from the literature. The travelling speed of holes and electrons are at 1×10^7 cm s⁻¹ [153]. This study employed the SCAPS-1D software to demonstrate the absorption coefficients pertaining to the ZnS and PEDOT:PSS as a HTL materials, while the absorption coefficient values pertaining to the PEDOT:PSS (HTL) materials and Sb₂Se₃ absorber are taken based on the literature [153].

| Properties | ZnS (ETL) | Sb ₂ Se ₃ | PEDOT: PSS (HTL) | References |
|---|----------------------|---------------------------------|----------------------|-----------------|
| Thickness (nm) | 70 | variable | 40 | [26, 154] |
| Bandgap, E _g (eV) | 3.5 | variable | 2.2 | [26, 153, 155] |
| Electron Affinity, χ_e (eV) | 4.5 | 4.04 | 2.9 | [156-158] |
| Dielectric permittivity, ϵ_r (relative) | 10 | 18 | 3 | [156, 159, 160] |
| Conduction band effective density of states, N _C (cm ⁻³) | 1.5×10^{18} | 2.2×10^{18} | 2.2×10^{15} | [157, 160, 161] |
| Valence band effective density of states, N _V (cm ⁻³) | 1.8×10^{18} | 1.8×10^{19} | 1.8×10^{18} | [157, 160, 161] |
| Electron thermal velocity (cm/s) | 1×10^7 | 1×10^7 | 1×10^7 | [152, 155, 159] |
| Hole thermal velocity | 1×10^7 | 1×10^7 | 1×10^7 | [152, 155, 159] |
| Electron mobility (cm ² /Vs) | 50 | 15 | 10 | [157, 160, 162] |
| Hole mobility (cm ² /Vs) | 20 | 5.1 | 10 | [157, 160, 162] |
| Shallow uniform donor density, N _D (cm ⁻³) | 1×10^{22} | 0 | 0 | [157] |

| | | | | |
|--|--------------------|----------|-----------------------|------------|
| Shallow uniform acceptor density, N_A (cm^{-3}) | 0 | variable | 3.17×10^{14} | [152, 157] |
| Defect density N_t (cm^{-3}) | 1×10^{14} | variable | 1×10^{16} | [152, 157] |
| Energy level | 0.6 | variable | 0.6 | [25] |

Table 3 A list of the several simulation variables used for the antimony triselenide.

3.1.2 Numerical simulation Method

As shown below, SCAPS-1D was used to solve Poisson's equation for electrons and holes (Equation 2)[163]:

$$\frac{d^2\psi}{dx^2} = \frac{e}{\epsilon_0\epsilon_r} [P(x) - n(x) + N_D - N_A + \rho_p - \rho_n] \quad (2)$$

Here, x denotes the electrostatic potential; ψ determines the elementary charge; ϵ_r denotes relative permittivity; ϵ_0 refers to the vacuum permittivity; p here represents concentration of holes and electrons. Donor and acceptor charges are denoted by N_D and N_A , respectively, and the concentration of holes and electrons is denoted by ρ_p and ρ_n . According to the theoretical viewpoint, the carrier lifespan τ has been defined as the time frame during which the charge carrier can move freely, allowing it to contribute to the electric conduction. Based on a uniform simulation of the Sb_2Se_3 , development of the G electron-hole pairs is done. Equation (2) and (3) define the developed electron and hole densities with regards to E_c and E_v , as represented below [164]:

$$\Delta n = G\tau_n \quad (2)$$

$$\Delta p = G\tau_p \quad (3)$$

The time spent on these traps was not considered in the τ_n and τ_p should the aforementioned carriers be thermally, and perovskite trapped. In terms of steady state, it was observed that, as shown in Equations (3) and (4) below, the rate of generation for the PSC was equal to the rate of trapping [164]:

$$\tau_n = \frac{1}{\sigma_p \cdot v_{th} \cdot (N_t - N_r)} \quad (4)$$

$$\tau_p = \frac{1}{\sigma_p \cdot v_{th} \cdot n_r} \quad (5)$$

Where occupied and unoccupied is denoted by (N_t) , occupied defects (n_r) , hole capture cross section σ_n and V_{th} refers to the thermal velocity respectively. As per Eqs. (4) and (5), the increase in defect density resulted in reduction in carrier lifetime as well as a short carrier diffusion Length (L)[165]. This L value accounted for the perovskite quality. It was seen that when there was higher L value versus perovskite thickness, the performance of the device can be enhanced. The following equations were constructed based on recombination current (J_0), L and V_{oc} :

$$J_0 \approx q \frac{Dn_i^2}{LN} \quad (6)$$

$$V_{oc} = \frac{KT}{q} \ln \left(\frac{J_{sc}}{J_0} + 1 \right) \quad (7)$$

With regard to equation (6) And (7), a decrease in the defect density resulted in reduction of recombination current as well as increase in V_{oc} , which was found to be comparable to the study results. The Internal Quantum Efficiency (IQE) and J_{sc} were observed to be directly proportional to each another. The IQE can depend on the minority carrier diffusion lengths, if the researchers consider the PSC to be a shallow junction solar cell along with a long minority carrier lifetime, as represented in Equation (8).

$$IQE = 1 - \alpha t - \frac{B}{\alpha L^2} \quad (8)$$

wherein α , t , and B indicated the spectral absorption coefficient, distance in the perovskite material and perovskite thickness, respectively[166]. We employed the Shockley-Read-Hall (SRH) recombination for describing the recombination components that impacted the defect density in the PSC, as represented below.

$$\mathfrak{R}^{SRH} = \frac{\vartheta \sigma_n \sigma_p N_T [np - n_i^2]}{\sigma_p [p + p_1] + \sigma_n [n + n_1]} \quad (9)$$

In this equation, ϑ stands for the thermal velocity of an electron, N_T for number of defects per volume, n_i for intrinsic number density, n & p for the concentration of electrons and holes at equilibrium. Here, n_1 denotes the concentration of electrons and p_1 denotes the concentration of holes in the trap defect and valence band. Hence, it was seen that the PSC was negatively impacted by the defect density. As per the researchers, increasing the absorber layer's thickness can solve this issue.

CHAPTER 4

RESULTS AND DISCUSSION

4.1 Effect of absorber layer thickness with QE

With the preliminary parameters from Table 3, Figure 17 displays the a) current density b) voltage characteristic and c) quantum efficiency (QE) achieved. Figure a) showed decline of Voc up to the ideal thickness of 200–800 nm, after which it showed no change. This shows that charge recombination rises in thicker films. Due to the incremental series resistance, FF first increases when the thickness reaches 200–800 nm and subsequently reduces from 84.14% to 83.99% when the thickness is further raised from 900–1100 nm. The simulation results are shown in Figure 17(b) as follows: When the absorber thickness is raised, the Jsc initially increases; when the thickness reaches its maximum at 1100 nm, it hits 44.95 mA/cm², saturating to a plateau. The ideal absorber thickness of 800 nm, or 28% PCE, is attained when the FF and Voc trends for various Sb₂Se₃ thicknesses are considered, as shown in Figure 15 (b). This is because a thin absorber does not benefit from complete light absorption, resulting in a low PCE. The photo-generated carriers will follow a longer transfer route, which results in increased recombination, if the absorber layer is too thick. The simulations that are in the dark demonstrate low current density and may be attributed to the minority carrier, when the Sb₂Se₃'s thickness is set to its ideal value of 800 nm. During the simulation, the reflection of the interface with each layer, as well as the series and shunt resistance, are not considered. The changes in the QE are shown in Figure 17(c): it includes the entire visible spectrum, has a high spectral response that extends from 300 to 900 nm, and has a large absorption start that rises to 500 nm. The shorter wavelength area is also caused by the absorber's subsequent parasitic absorption.

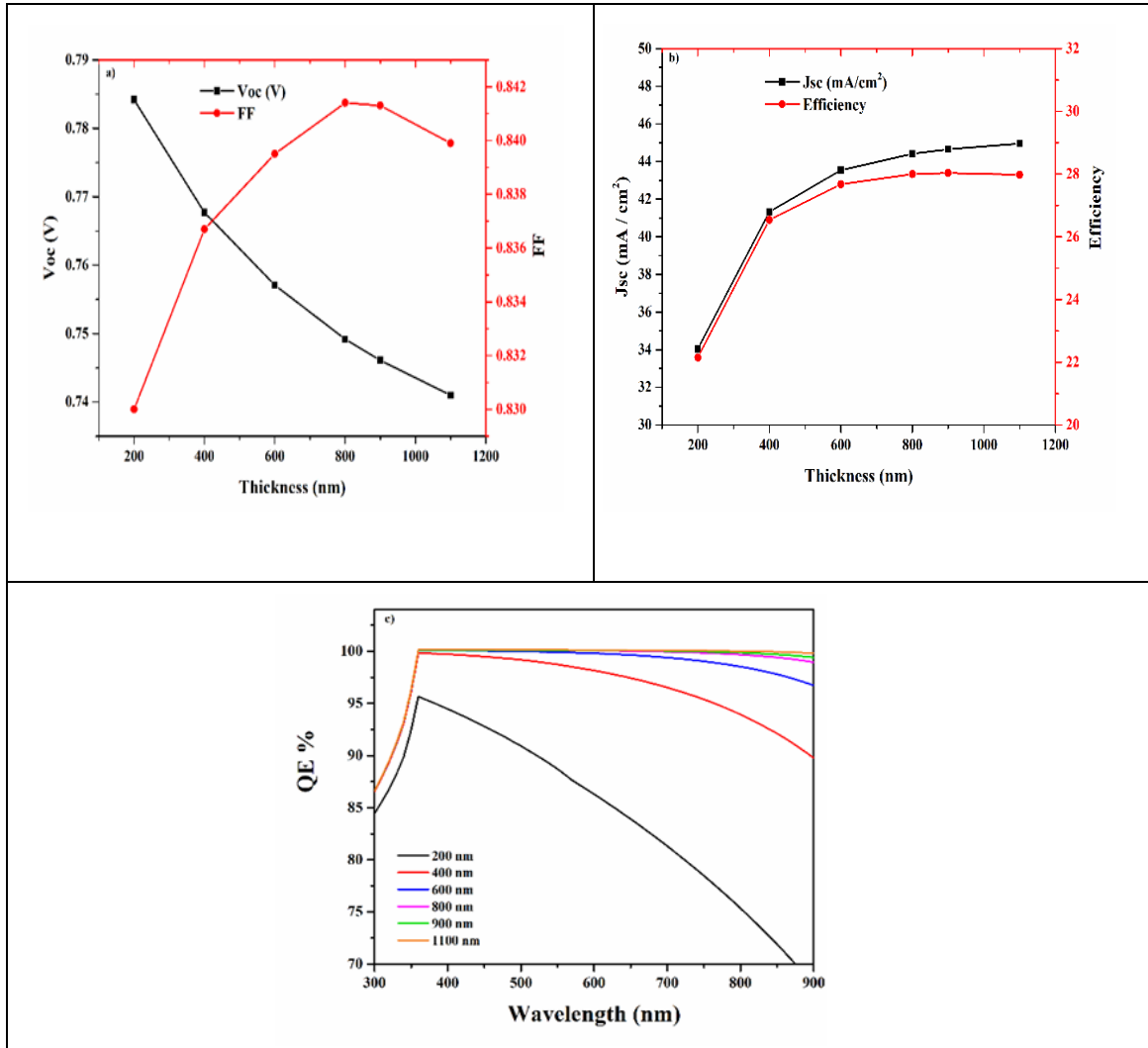


Figure 17 Absorber layer thicknesses with a) open-circuit voltage & fill factor b); J_{sc} and Efficiency, c) ;Quantum efficiency

4.2 Effect of absorber layer Carrier concentration and bandgap

This section focuses on elucidating the influence of absorber layers on photovoltaic performance characteristics, which ultimately dictate the efficiency of solar cell conversion. Figure 18 illustrates that as the bandgap increases, JSC decreases while VOC, which is directly related to bandgap, increases. A higher bandgap results in an increase in VOC and a reduction in the rate of radiative recombination [167]. On the other hand, JSC undergoes significant changes, ranging from 30 to 46 (mA/cm^2) as shown in Figure 18. At low concentrations, there is reduced carrier collection at the front contact, leading to a decrease in JSC [168].

Nonetheless, a high JSC value can be maintained by using a buffer layer with a higher carrier concentration. However, in our scenario, even with a higher carrier concentration, no noticeable improvement is observed, which could be explained by optimal band alignment at the buffer/absorber interface with increased carrier concentration and bandgap. Such alignment is crucial for efficient solar cells in increasing JSC possibly due to enhanced diffusivity of carriers resulting from increased mobility[169]. Alternatively, because of a widening bandgap and constant carrier concentration, FF decreases. PCE showed improvement at the absorber layer's higher bandgap despite the higher carrier concentration's influence and although PCE is the function of FF, V_{oc} , and J_{sc} . Our findings demonstrate that the optimal performance began at a 1.2 eV bandgap and a 1×10^{16} ($1/\text{cm}^3$) defect density.

Improper definition and adjustment of the optical qualities of the connected absorber layer can lead to inaccurate predictions regarding the real potential of the examined p-absorber material [170]. For instance, let us consider the example of examining Sb_2Sb_3 , which has a 1.04 eV band gap. Due to the material's polycrystalline nature and the process of non-optimized deposition, it is highly probable that the absorber layer's thin film will already have a bulk defect density during the early phases of the design process. In such a situation, the assembled absorber layer would exhibit a low carrier concentration, and it is possible that the associated device's efficacy would be below 24% (as depicted in Figure 18 d). However, the device's efficiency could be enhanced even further by utilizing an absorber layer with a greater carrier concentration.

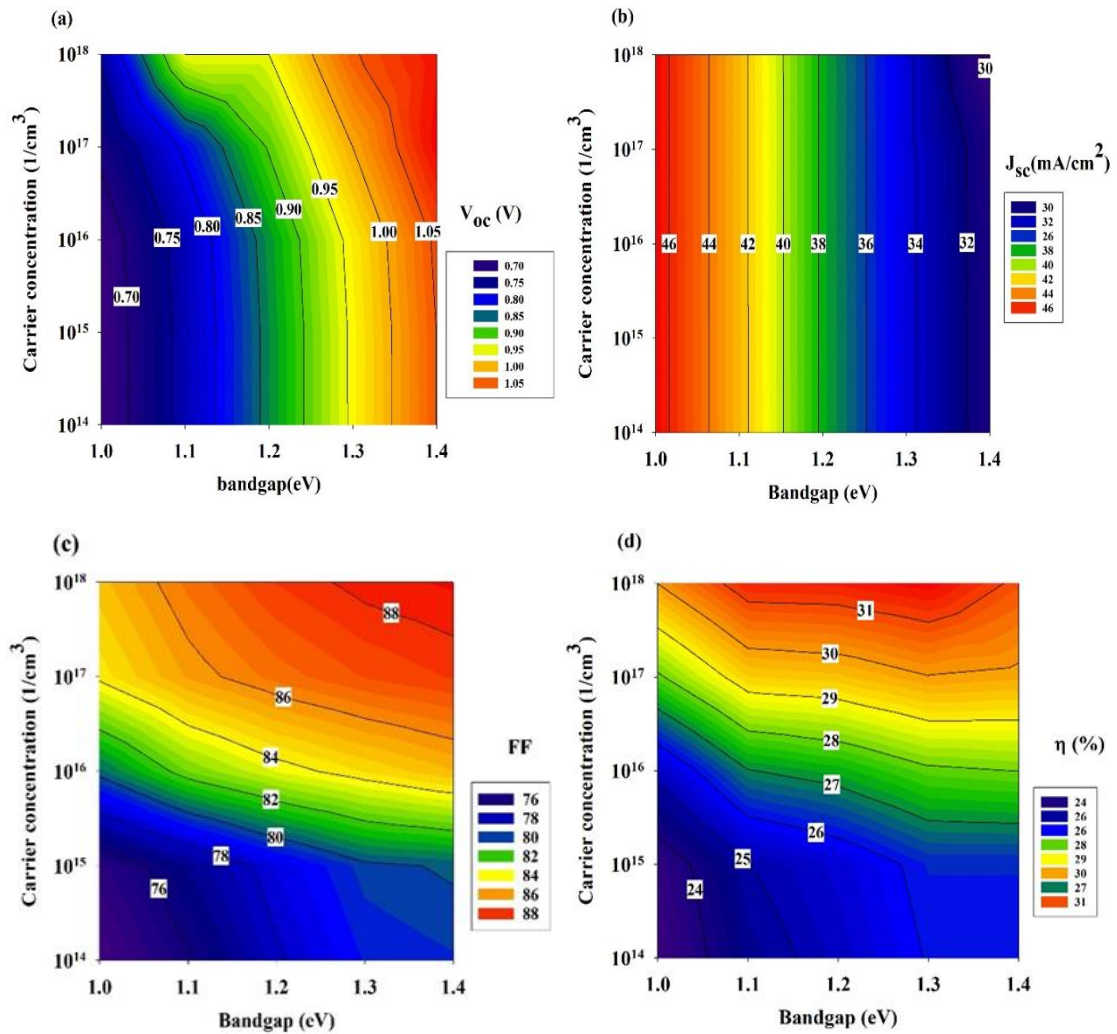


Figure 18 Photovoltaic performance parameters at various carrier concentrations

4.3 Defect density vs energy level

The defect density of the absorber layer is a crucial characteristic that can significantly impact the performance of a device. Higher concentrations of defects in the absorber layer can lead to a greater rate of recombination due to the growth of pinholes, as well as a higher rate of film degradation, a lower strength, and a decrease in the device's overall performance [167]. On the other hand, a low defect density can enhance the length of carrier diffusion and reject the recombination process, leading to improved PV performance. Figure 19 (a-d) depicts the effect of absorber layer

defect density on the most significant parameters by modifying the defect density from $1 \times 10^{14} \text{ cm}^{-3}$ to $1 \times 10^{18} \text{ cm}^{-3}$. It is evident that cell performance deteriorates as the overall defect density of the absorber layer increases. The defect density is an essential parameter that affects the cell's performance, and it has a substantial impact on FF, VOC, and JSC.

The impact of radiative recombination on electron-hole pair formation and passage in solar cells was found to be minor and modifying the JSC defect states had little effect until it reached around $1 \times 10^{17} \text{ cm}^{-3}$. The existence of defect energy levels was responsible for significant changes in Voc, ranging from 0.6 to 1.0 V, which were clearly observable. However, the effect of radiative recombination on FF was more distinct, as an increase in radiative recombination rate led to a decline in FF. This decline was due to a less effective transportation of electron-hole pairs through the cell, resulting in an increase in the energy quantity lost to recombination [168]. For instance, at 0.55 eV energy level, the FF is as low as $\sim 65\%$ with a defect density of $1 \times 10^{18} \text{ cm}^{-3}$ and it increases to 85% when the defect density is below $1 \times 10^{14} \text{ cm}^{-3}$. Moreover, as the defect density increases from $1 \times 10^{14} \text{ cm}^{-3}$ to $1 \times 10^{18} \text{ cm}^{-3}$, the efficiency declines drastically, the decline being between 10% and 30% [as shown in Figure 19 (d)].

In conclusion, it can be stated that the defect density has a direct impact on the efficiency of the cell. As the number of defects increases, the charge carrier diffusion length decreases, leading to the introduction of more recombination carriers to the absorber layer. This, in turn, results in a higher recombination rate, ultimately affecting the cell's performance. The optimal efficiency of the cell, i.e., 30%, can be achieved by fine-tuning the VOC at 1.0 eV, the JSC at 34 mA/cm^2 , FF at 85%, and maintaining the defect density at $1 \times 10^{14} \text{ cm}^{-3}$ [169].

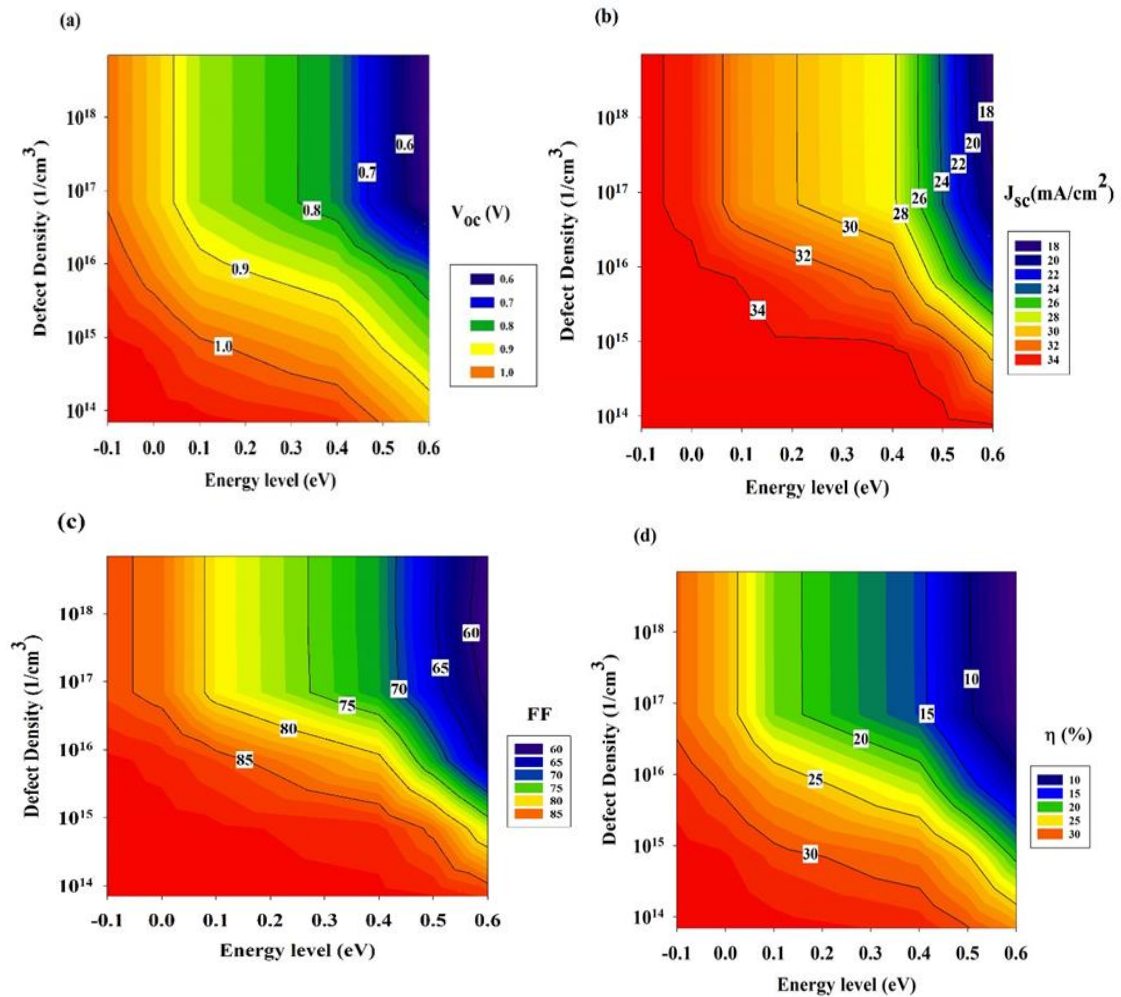


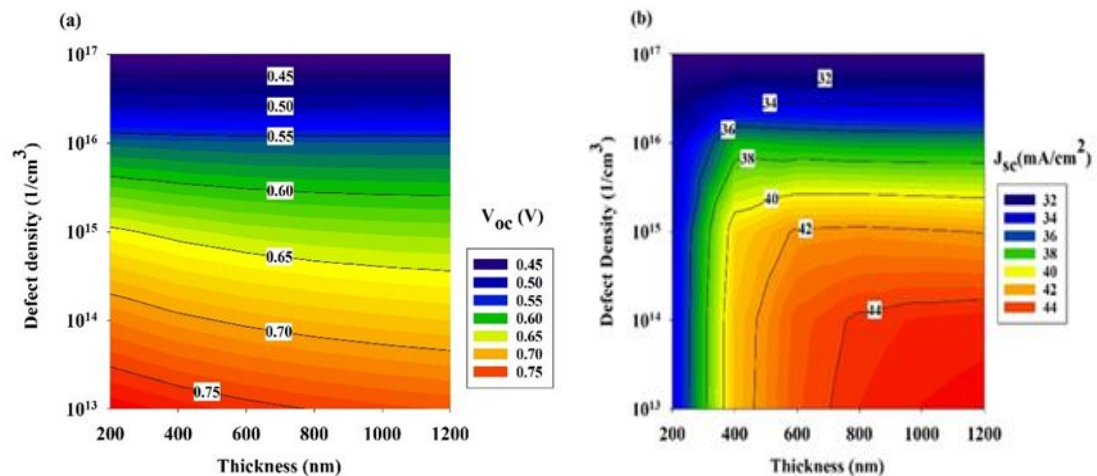
Figure 19 Photovoltaic performance parameters at various defect densities

4.4 Effect of defect density of the absorption layer on the antimony cell performance

Figure 16 shows the equilibrium band diagram of the p-i-n Sb_2Se_3 solar cell. The absorber layer has 0.6 eV defect energy, lower than the conduction band. Figure 20 shows Sb_2Se_3 solar cell performance metrics, absorber defect density, and layer thickness. Deep-defect density and absorber layer thickness affect device performance (ranging between 10^{13} and 10^{17} cm^{-3} ; 200 and 1200 nm, respectively). Fault density reduced device performance as V_{oc} ranged from 0.73 to 0.778 V. At defect densities of 10^{13} cm^{-3} and layer thicknesses of 200 nm, the maximum V_{oc} value of 0.79 V was observed. V_{oc} was also found to drop precipitously to 0.778 at defect concentrations of $>10^{13}$ and absorber layer thicknesses of >200 nm, before dropping continuously to

a value of 0.73 V. At a layer thickness of 800 nm and a defect density of 10^{14} cm^{-3} , the peak J_{sc} was measured to be $>44 \text{ mA/cm}^2$.

The graph revealed that if the thickness value was lowered from 600 nm to 200 nm, the J_{sc} dropped from 43 mA/cm^2 to 32 mA/cm^2 . The same pattern was seen for defect densities greater than 10^{15} cm^{-3} . The value of FF is diminished by processes like Voc and recombination [171]. At a defect density of 10^{14} cm^{-3} , the results showed that the FF value was greater than 80%. The thickness value has no bearing on this. The efficiency was defined by the researchers using the $\text{PCE} = \text{Voc}, J_{sc}, \text{FF}$ equations, which consider all three output properties simultaneously. We found that a PCE of $>25\%$ was achieved at a thickness value of $>900 \text{ nm}$ and a defect density of 10^{13} cm^{-3} . Earlier research [9, 12] showed that the efficiency of the Sb_2Se_3 film may be increased if it were developed in a [001] direction, perpendicular to the p-n junction contact. Conversely, it was shown that a defect density of $>10^{15} \text{ cm}^{-3}$ resulted in a considerable performance loss of 10-15%, and that the PCE went down to 20% when the layer thickness was below 900 nm.



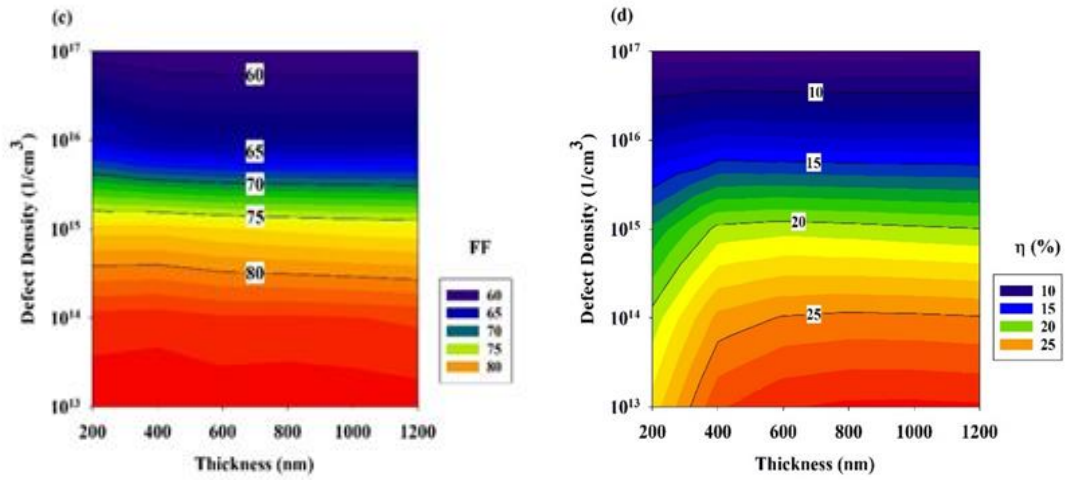


Figure 20 Performance of the PSC as a function of parameters like absorber defect density and layer thickness shown using contour graphs.

4.5 Effect of the interface defect density on the PSC performance

The performance of the device is affected by various ZnS/Sb₂Se₃ layer interfacial defects, as shown in Figure 21. The ZnS layer's value was greater than the energy level at 0.6 eV. This component also revealed the same pattern as before. But over time, the system's susceptibility to flaws increased. The fault density dropped from 10¹⁴ cm⁻³ to 10¹¹ cm⁻³, as evidenced by the data. When the absorber thickness was 700 nm and the interface defect density was 10¹¹ cm⁻³, a value of 0.75 V was observed in a tiny area. At greater than 10¹⁵ cm⁻³, the Voc dropped to 0.95 V beyond this range. It was also observed that the Jsc increased from 22 to 27 mA/cm² when the absorber thickness grew from 300 to 1000 nm and that it was not defect density sensitive. The researchers found that while a fault concentration of >10¹³ cm⁻³ might reduce the FF by 50%, the thickness of the absorber layer did not significantly alter the FF value. Finally, if the thickness was greater than 700 nm and the defect densities were greater than 10¹¹ cm⁻³, respectively, a maximum PCE of 28% was recorded. Based on the research, it was determined that light absorption was responsible for a greater series resistance at the ZnS/absorber contact. This improved the performance of the ZnS film based Sb₂Se₃ solar cells by increasing the effective and electrical dissociation of the excitons and transport charge carriers [51]. This was attributed to

the metal cations diffusing across the Sb_2Se_3 as it developed. Major interfacial deformations occurred because of the multiple structural issues in the various materials, which caused charge recombination in the solar cell devices.

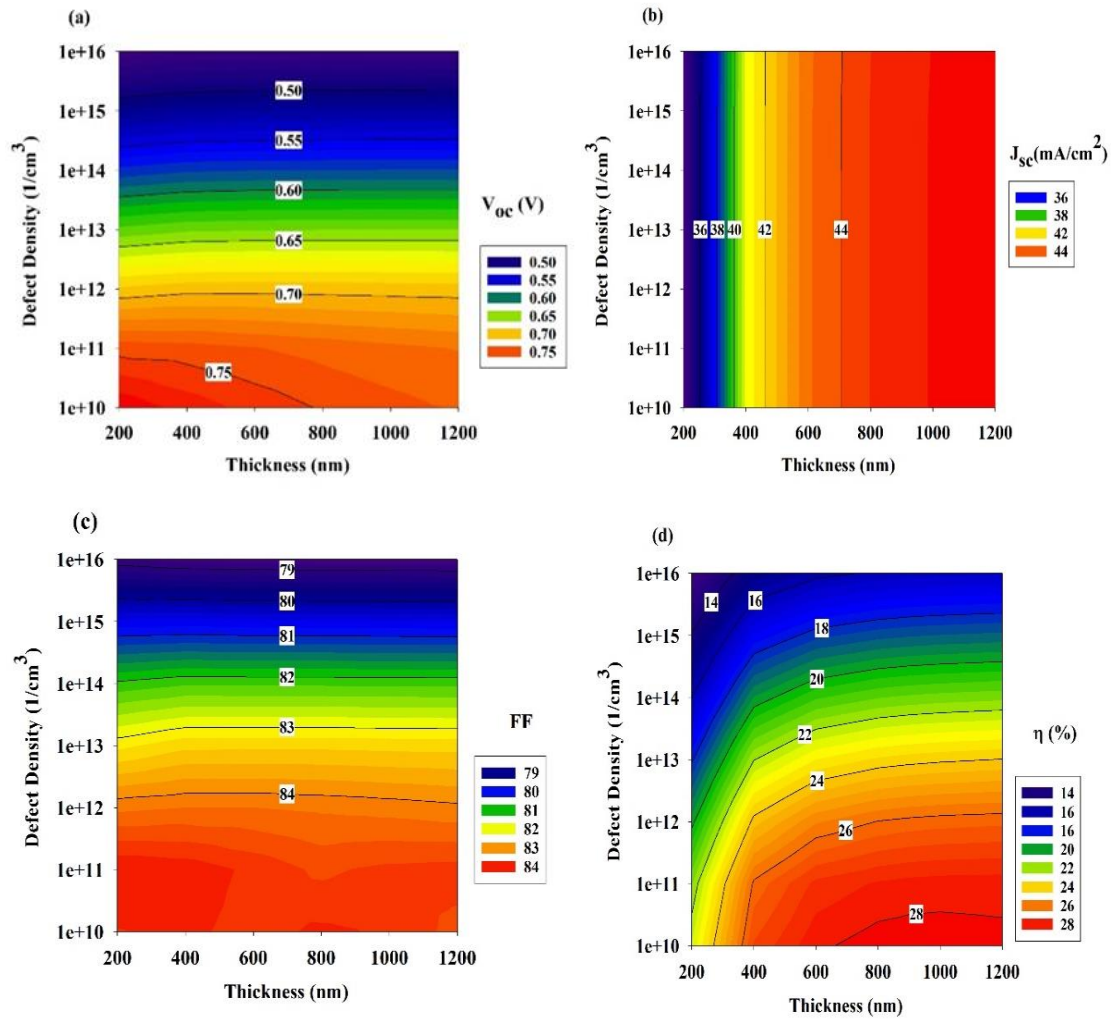


Figure 21 Shows contour graphs that show the PSC performance in relation to variables like the defect density at the ZnS/Antimony Triselenide Interface and the thickness of the Antimony Triselenide Layer.

4.6 Effect of electron affinity with bandgap

Sb_2S_3 is a promising material for single-junction solar cells due to its favorable electronic properties and wide bandgap. However, the highest power conversion efficiency achieved for Sb_2S_3 -based solar cells so far falls short of more advanced

thin-film technologies. Tandem devices incorporating Sb_2S_3 as the top cell and a low bandgap bottom cell could overcome this efficiency limitation and enable highly effective light conversion. Further research is needed to optimize the properties and performance of Sb_2S_3 -based solar cells, especially in tandem configurations, for practical applications in renewable energy systems.[74].

The optical properties of antimony tri-selenide (Sb_2Se_3) are strongly influenced by its chemical composition and crystal structure, which can vary depending on the deposition method and growth conditions used to produce thin films. As a result, the reported band gap values for polycrystalline Sb_2Se_3 thin films range from 1.0 eV to 1.3 eV [16]. However, both experimental and theoretical evidence suggests that the band gap of Sb_2Se_3 falls within the ideal range for solar cell applications [172]. At 300 K, Sb_2Se_3 has a direct band gap of 1.17 eV and an indirect band gap of 1.03 eV. To maximize the efficiency of a solar cell, the band gap of the material used for the absorber layer should be well-suited to the spectrum of solar radiation, allowing for the absorption of as many photons as possible. If the band gap is too large, some photons will pass through the material without generating an electron-hole pair. The band gap of Sb_2Se_3 can be narrowed by increasing the annealing temperature during the thin film deposition process.

The open circuit voltage is seen increasing with increasing bandgap and electron affinity whereas short circuit current decreases when the band gap is at 1.1 eV as shown in figure 22. When the bandgap and electron affinity increase, the energy required for electron-hole pairs to recombine and release energy in the form of photons decreases. This leads to a reduction in the recombination rate of charge carriers, resulting in an increase in the V_{oc} of the solar cell. At the same time, the short circuit current decreases with increasing bandgap due to a decrease in the number of available electron-hole pairs. This is because the probability of photon absorption decreases as the bandgap increases, leading to a decrease in the number of available electrons and holes for current generation. Therefore, the reduction in available carriers leads to a decrease in I_{sc} . It can be concluded that the increase in bandgap and electron affinity of a solar cell material leads to an increase in V_{oc} due

to a reduction in the recombination rate of charge carriers, but a decrease in J_{sc} due to a reduction in the number of available electron-hole pairs.

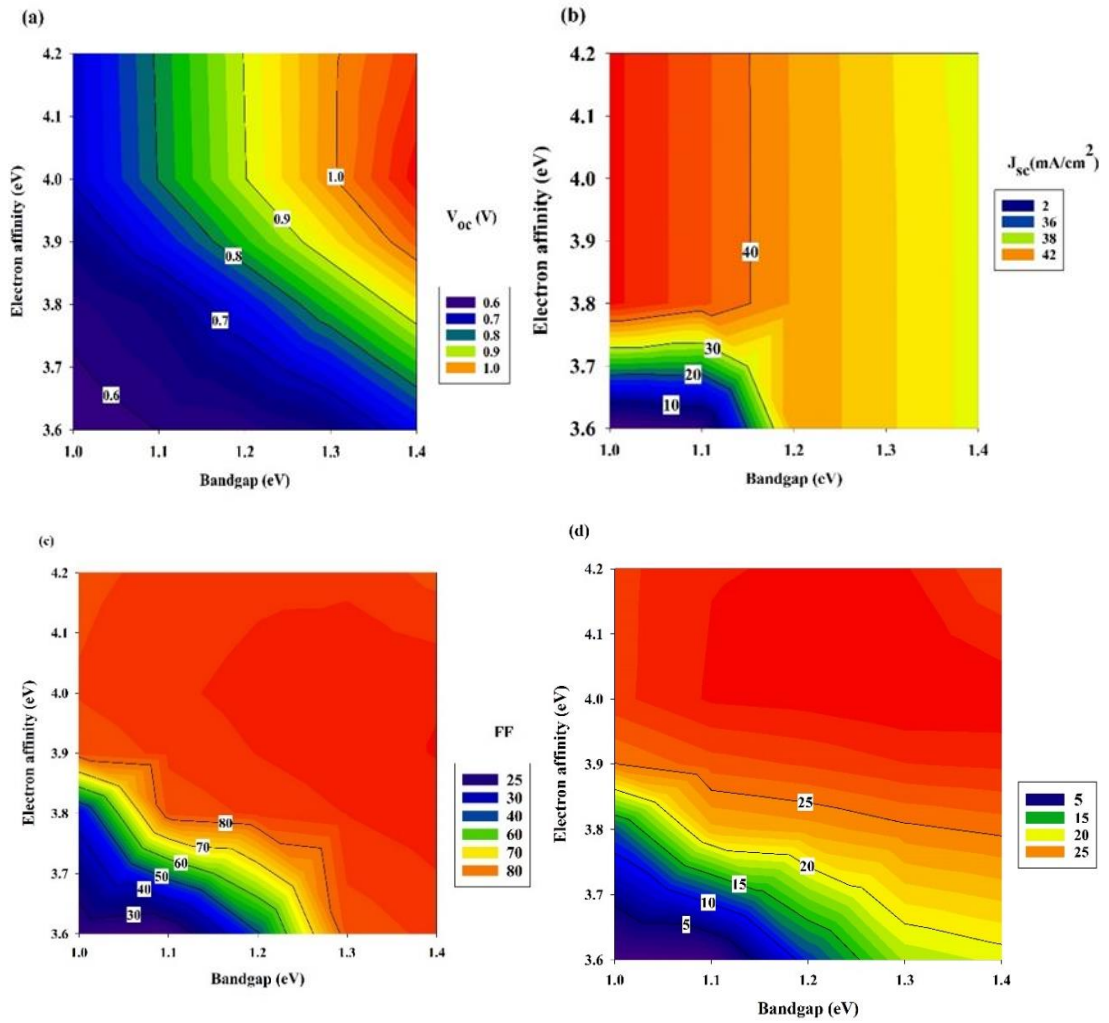


Figure 22 Effect of electron affinity with bandgap

CHAPTER 5

CONCLUSION AND FUTURE PROSPECTS

In this research, the development of antimony triselenide solar cells was optimized using the SCAPS 1-D simulator for the p-i-n arrangement. The primary solar cell was designed based on the TCO/ZnS/ Sb₂Se₃/PEDOT: PSS arrangement, and various parameters were optimized, including the absorber layer thickness (ranging from 200 to 1100 nm), carrier concentration (ranging from 10¹⁴ to 10¹⁸ cm⁻³), defect density (ranging from 10¹⁴ to 10¹⁸ cm⁻³), and energy level (ranging from -0.1 to 0.6 eV). The simulations showed that the optimized solar cell design achieved a PCE of over 30%, with a Voc of 1.0 eV, Jsc of 34 mA/cm², and FF of 85%. Furthermore, it was observed that the efficiency of the antimony triselenide solar cells improved as the thickness of the absorber layer increased.

The study found that for optimal device performance, the Sb₂Se₃ absorber layer should have a thickness of 800nm, a bandgap of 1.2 eV, and a carrier concentration of 10¹⁴ cm⁻³. The impact of absorber layer thickness and quantum efficiency on device performance was also examined, with varying values for defect density (ranging from 10¹⁴ to 10¹⁸ cm⁻³), energy level (ranging from -0.1 to 0.6 eV), and absorber layer thickness (ranging from 200 to 1100 nm). Results showed that a defect density less than 10¹⁵ cm⁻³, an energy level of 0.1 eV above the valence band, and an optimal bandgap of 1.2 eV are necessary for optimal performance. The highest efficiency of 30% was achieved through the optimization of various parameters. These simulation results provide valuable insights and directions for the design and engineering of Sb₂Se₃ solar cells. Additionally, the performance of the device was highly influenced by defect densities and absorber layer thickness, although a similar pattern was observed in the latter case. Increasing the absorber layer thickness from 300 nm to 900 nm led to a significant increase in PCE, but a slight drop was observed when it was further increased from 1000 nm to 1100 nm.

The research results have significant implications for enhancing the design of Sb₂Se₃ solar cells and could lead to their widespread commercialization, potentially replacing silicon-based solar cells in the future. This study could drive further

research on antimony triselenide solar cells to improve their effectiveness and reduce their cost. The identified optimal parameters, including absorber layer thickness and defect density, could serve as a model for future investigations to enhance their performance. Additionally, the findings may inspire the creation of new materials or designs for more efficient and affordable solar cells. Overall, this study's insights could have significant implications for sustainable and renewable energy sources.

Based on the conclusion of the study, there are several potential prospects for the development and optimization of Sb₂Se₃ solar cells. Here are a few suggestions:

- i. Further optimization of device parameters: The study showed that optimizing the absorber layer thickness, carrier concentration, defect density, and energy level can significantly improve the efficiency of antimony triselenide solar cells. Future research could focus on optimizing these parameters further to achieve even higher efficiency levels.
- ii. Exploration of new materials and device structures: While the p-i-n arrangement was used in this study, there may be other device structures or materials that could be used to improve the performance of antimony triselenide solar cells. Future research could explore alternative device structures or other semiconductor materials to determine if they could offer higher efficiencies or better stability.
- iii. Scale-up of manufacturing processes: To bring antimony triselenide solar cells to market, it will be necessary to scale up the manufacturing processes. Future research could focus on developing scalable fabrication methods that can produce high-quality devices at a reasonable cost.
- iv. Improved stability and durability: For antimony triselenide solar cells to be commercially viable, they must demonstrate long-term stability and durability. Future research could focus on improving the stability and durability of these devices, so they can withstand harsh environmental conditions and last for many years without degradation.

REFERENCE

1. John, H., Electrical Characterization of Photo voltaic Materials and Solar Cells with the Model 4200-SCS Semiconductor Characterization System. Application Note Series, Keithley Instruments, Inc, USA, 2011.
2. Wang, W., et al., Interface etching leads to the inversion of the conduction band offset between the CdS/Sb₂Se₃ heterojunction and high-efficient Sb₂Se₃ solar cells. ACS Applied Energy Materials, 2022. **5**(2): p. 2531-2541.
3. Liang, G., et al., Crystal Growth Promotion and Defects Healing Enable Minimum Open-Circuit Voltage Deficit in Antimony Selenide Solar Cells. Advanced Science, 2022. **9**(9): p. 2105142.
4. Wang, W., et al., Over 6% certified Sb₂(S, Se)₃ solar cells fabricated via in situ hydrothermal growth and postselenization. Advanced Electronic Materials, 2019. **5**(2): p. 1800683.
5. Chen, S., et al., Magnetron sputtered Sb₂Se₃-based thin films towards high performance quasi-homojunction thin film solar cells. Solar Energy Materials and Solar Cells, 2019. **203**: p. 110154.
6. Guillermo, H., et al., A simple model for studying the effects of activation treatment on the defects structure of cadmium telluride solar cells. Optik, 2022: p. 169296.
7. Kaelin, M., D. Rudmann, and A. Tiwari, Low cost processing of CIGS thin film solar cells. Solar Energy, 2004. **77**(6): p. 749-756.
8. Islam, M.M., et al., CIGS solar cell with MBE-grown ZnS buffer layer. Solar energy materials and solar cells, 2009. **93**(6-7): p. 970-972.
9. Bouich, A., et al., Tetrabutylammonium (TBA)-Doped Methylammonium Lead Iodide: High Quality and Stable Perovskite Thin Films. Front. Energy Res, 2022. **10**: p. 840817.
10. Wong, L.H., et al., Emerging inorganic solar cell efficiency tables (Version 1). Journal of Physics: Energy, 2019. **1**(3): p. 032001.
11. Karade, V.C., et al., Combating open circuit voltage loss in Sb₂Se₃ solar cell with an application of SnS as a back surface field layer. Solar Energy, 2022. **233**: p. 435-445.

12. Rijal, S., et al., Templated Growth and Passivation of Vertically Oriented Antimony Selenide Thin Films for High-Efficiency Solar Cells in Substrate Configuration. *Advanced Functional Materials*, 2022. **32**(10): p. 2110032.
13. Zhou, Y., et al., Solution-processed antimony selenide heterojunction solar cells. *Advanced Energy Materials*, 2014. **4**(8): p. 1301846.
14. Ko, T.-Y., M. Shellaiah, and K.W. Sun, Thermal and thermoelectric transport in highly resistive single Sb₂Se₃ nanowires and nanowire bundles. *Scientific reports*, 2016. **6**(1): p. 1-9.
15. Singh, Y., K. Maurya, and V. Singh, A review on properties, applications, and deposition techniques of antimony selenide. *Solar Energy Materials and Solar Cells*, 2021. **230**: p. 111223.
16. Mavlonov, A., et al., A review of Sb₂Se₃ photovoltaic absorber materials and thin-film solar cells. *Solar Energy*, 2020. **201**: p. 227-246.
17. Liu, X., et al., Enhanced open circuit voltage of Sb₂Se₃/CdS solar cells by annealing Se-rich amorphous Sb₂Se₃ films prepared via sputtering process. *Solar Energy*, 2020. **195**: p. 697-702.
18. Chen, C., et al., 6.5% certified efficiency Sb₂Se₃ solar cells using PbS colloidal quantum dot film as hole-transporting layer. *ACS Energy Letters*, 2017. **2**(9): p. 2125-2132.
19. Ren, D., et al., Structure, morphology, and photoelectric performances of Te-Sb₂Se₃ thin film prepared via magnetron sputtering. *Nanomaterials*, 2020. **10**(7): p. 1358.
20. Daboczi, M., et al., Origin of open-circuit voltage losses in perovskite solar cells investigated by surface photovoltage measurement. *ACS applied materials & interfaces*, 2019. **11**(50): p. 46808-46817.
21. Li, Z., et al., 9.2%-efficient core-shell structured antimony selenide nanorod array solar cells. *Nature communications*, 2019. **10**(1): p. 1-9.
22. Reza, K.M., S. Mabrouk, and Q. Qiao, A review on tailoring PEDOT: PSS layer for improved performance of perovskite solar cells. *Proc. Nat. Res. Soc*, 2018. **2**(1): p. 02004.

23. Du, T., et al., p-Doping of organic hole transport layers in p–i–n perovskite solar cells: correlating open-circuit voltage and photoluminescence quenching. *Journal of Materials Chemistry A*, 2019. **7**(32): p. 18971-18979.
24. Benami, A., et al., Comparison of the Effects of ZnO and TiO₂ on the Performance of Perovskite Solar Cells via SCAPS-1D Software Package. 2022.
25. Khac, D.L., et al., Influence/Effect of Deep-Level Defect of Absorber Layer and n/i Interface on the Performance of Antimony Triselenide Solar Cells by Numerical Simulation. *Sustainability*, 2022. **14**(11): p. 6780.
26. Zheng, E., et al., ZnO/ZnS core-shell composites for low-temperature-processed perovskite solar cells. *Journal of energy chemistry*, 2018. **27**(5): p. 1461-1467.
27. Chin, Y.-C., et al., Suppressing PEDOT: PSS doping-induced interfacial recombination loss in perovskite solar cells. *ACS energy letters*, 2022. **7**(2): p. 560-568.
28. Qin, M., et al., Perovskite solar cells based on low-temperature processed indium oxide electron selective layers. *ACS applied materials & interfaces*, 2016. **8**(13): p. 8460-8466.
29. Zhao, X., et al., Interface engineering in 1D ZnO-based heterostructures for photoelectrical devices. *Advanced Functional Materials*, 2022. **32**(11): p. 2106887.
30. Logan, M., The closing window: inadequate progress on climate action makes rapid transformation of societies only option, finds UN report. 2022.
31. Tazeen, H., Impact of agriculture on deforestation. *International Journal of Modern Agriculture*, 2021. **10**(2): p. 2940-2947.
32. Kumar, N.H., et al., Impact of climate change on biodiversity and shift in major biomes, in *Global Climate Change*. 2021, Elsevier. p. 33-44.
33. Harris, J.M. and B. Roach, *Ecological economics: Basic concepts*, in *Environmental and Natural Resource Economics*. 2021, Routledge. p. 225-249.
34. Kirsch, S., Running out? Rethinking resource depletion. *The Extractive Industries and Society*, 2020. **7**(3): p. 838-840.

35. Murdock, H.E., et al., Renewables 2021-Global status report. 2021.
36. Husain, A.A., et al., A review of transparent solar photovoltaic technologies. Renewable and sustainable energy reviews, 2018. **94**: p. 779-791.
37. Gielen, D., et al., Global energy transformation: a roadmap to 2050. 2019.
38. Newell, R., et al., Global energy outlook 2021: Pathways from Paris. Resources for the Future, 2021. **8**.
39. Chakraborty, S., J. Li, and P. Bhattacharya, The solution to the global energy crisis with new materials, and sustainability. Journal of Phase Change Materials, 2021. **1**(2).
40. Bashir, R., et al., Comparative study of the photovoltaic behavior of ruthenium and the other organic and inorganic Dye-Sensitized Solar Cells (DSSC). Optik, 2018. **157**: p. 11-15.
41. Qamhie, N., et al., Synthesis and characterization of a perovskite film for solar cells applications. Optik, 2018. **171**: p. 648-651.
42. Opeyemi, O., et al., Porphyrin and phthalocyanines-based solar cells: fundamental mechanisms and recent advances. Advanced Journal of Chemistry-Section A, 2019. **2**(1): p. 21-44.
43. Dubey, R.S. and S. Saravanan, Ultrathin Film Amorphous Silicon Solar Cell Performance using Rigorous Coupled Wave Analysis Method. International Journal of Renewable Energy Development.
44. Abbas, S., et al., Numerical Simulation of the Performance of Sb₂Se₃ Solar Cell via Optimizing the Optoelectronic Properties Based SCAPS-1D. Materials, 2022. **15**(18): p. 6272.
45. Soley, S. and A. Dwivedi. Advances in high efficiency crystalline silicon homo junction solar cell technology. in AIP conference proceedings. 2019. AIP Publishing LLC.
46. Alharbi, F.H. and S. Kais, Theoretical limits of photovoltaics efficiency and possible improvements by intuitive approaches learned from photosynthesis and quantum coherence. Renewable and Sustainable Energy Reviews, 2015. **43**: p. 1073-1089.

47. Pham, H.D., et al., Development of dopant-free organic hole transporting materials for perovskite solar cells. *Advanced Energy Materials*, 2020. **10**(13): p. 1903326.
48. Rathore, N., et al., A comprehensive review of different types of solar photovoltaic cells and their applications. *International Journal of Ambient Energy*, 2021. **42**(10): p. 1200-1217.
49. Kibria, M.T., et al. A Review: Comparative studies on different generation solar cells technology. in *Proc. of 5th International Conference on Environmental Aspects of Bangladesh*. 2014.
50. Bagher, A.M., M.M.A. Vahid, and M. Mohsen, Types of solar cells and application. *American Journal of optics and Photonics*, 2015. **3**(5): p. 94-113.
51. Kichou, S., et al., Analysis of the behaviour of cadmium telluride and crystalline silicon photovoltaic modules deployed outdoor under humid continental climate conditions. *Solar Energy*, 2018. **171**: p. 681-691.
52. Parida, B., S. Iniyam, and R. Goic, A review of solar photovoltaic technologies. *Renewable and sustainable energy reviews*, 2011. **15**(3): p. 1625-1636.
53. Tang, R., et al., Highly efficient and stable planar heterojunction solar cell based on sputtered and post-selenized Sb₂Se₃ thin film. *Nano Energy*, 2019. **64**: p. 103929.
54. Lai, K.-K., et al., A structured MPA approach to explore technological core competence, knowledge flow, and technology development through social network patentometrics. *Journal of Knowledge Management*, 2021. **25**(2): p. 402-432.
55. Soufiani, A.M., et al., Polaronic exciton binding energy in iodide and bromide organic-inorganic lead halide perovskites. *Applied Physics Letters*, 2015. **107**(23): p. 231902.
56. Grätzel, M., The light and shade of perovskite solar cells. *Nature materials*, 2014. **13**(9): p. 838-842.
57. Gorella, N., Characterization of as prepared and exposed Perovskite solar cells by microscopic and spectroscopic techniques. 2021.

58. Singhal, n., numerical simulation of pcbm and moo3 staced electron and hole transport layer based perovskite solar cell. 2018.
59. Kumar, N.S. and K.C.B. Naidu, A review on perovskite solar cells (PSCs), materials and applications. *Journal of Materiomics*, 2021. **7**(5): p. 940-956.
60. D'Innocenzo, V., et al., Tuning the light emission properties by band gap engineering in hybrid lead halide perovskite. *Journal of the American Chemical Society*, 2014. **136**(51): p. 17730-17733.
61. Dharmadasa, I.M., "Advanced Thin Film Materials for Photovoltaic Applications". 2020, MDPI. p. 562.
62. Kojima, A., et al., Organometal halide perovskites as visible-light sensitizers for photovoltaic cells. *Journal of the american chemical society*, 2009. **131**(17): p. 6050-6051.
63. Nie, W., et al., High-efficiency solution-processed perovskite solar cells with millimeter-scale grains. *Science*, 2015. **347**(6221): p. 522-525.
64. Fournier, O., et al., Interfacial tuning of hybrid halide triple cation perovskite solar cells with inorganic electron transport layer.
65. Lee, J., K.F. Mak, and J. Shan, Electrical control of the valley Hall effect in bilayer MoS₂ transistors. *Nature nanotechnology*, 2016. **11**(5): p. 421-425.
66. Dasgupta, U., S. Chatterjee, and A.J. Pal, Thin-film formation of 2D MoS₂ and its application as a hole-transport layer in planar perovskite solar cells. *Solar Energy Materials and Solar Cells*, 2017. **172**: p. 353-360.
67. Abd Malek, N.A., et al., Ultra-thin MoS₂ nanosheet for electron transport layer of perovskite solar cells. *Optical Materials*, 2020. **104**: p. 109933.
68. Chu, Q.-Q., et al., Highly stable carbon-based perovskite solar cell with a record efficiency of over 18% via hole transport engineering. *Journal of Materials Science & Technology*, 2019. **35**(6): p. 987-993.
69. Kim, D.I., et al., Oxygen-plasma processed Spiro-OMeTAD toward high performance for perovskite solar cell. *Surface and Coatings Technology*, 2019. **357**: p. 189-194.
70. Xing, G. and N. Mathews, S, Sun, SS Lim, YM Lam, M. Grätzel, S. Mhaisalkar, and T. C. Sum. *Science*, 2013. **342**(6156): p. 344-347.

71. Peng, G., X. Xu, and G. Xu, Hybrid organic-inorganic perovskites open a new era for low-cost, high efficiency solar cells. *Journal of Nanomaterials*, 2015. **2015**.
72. Zeng, K., D.-J. Xue, and J. Tang, Antimony selenide thin-film solar cells. *Semiconductor Science and Technology*, 2016. **31**(6): p. 063001.
73. Singh, Y., K. Maurya, and V. Singh, n-Si/p-Sb₂Se₃ structure based simple solar cell device. *Materials Today Sustainability*, 2022. **18**: p. 100148.
74. Shah, U.A., et al., Wide bandgap Sb₂S₃ solar cells. *Advanced Functional Materials*, 2021. **31**(27): p. 2100265.
75. Kondrotas, R., C. Chen, and J. Tang, Sb₂S₃ solar cells. *Joule*, 2018. **2**(5): p. 857-878.
76. Khan, M.D., et al., Novel single source precursor for synthesis of Sb₂Se₃ nanorods and deposition of thin films by AACVD: Photo-electrochemical study for water reduction catalysis. *Solar Energy*, 2018. **169**: p. 526-534.
77. Liang, G.-X., et al., Sputtered and selenized Sb₂Se₃ thin-film solar cells with open-circuit voltage exceeding 500 mV. *Nano Energy*, 2020. **73**: p. 104806.
78. Soonmin, H., et al., Recent Developments on the Properties of Chalcogenide Thin Films. 2022.
79. Luo, W., et al., Ultralong Sb₂Se₃ nanowire-based free-standing membrane anode for lithium/sodium ion batteries. *ACS Applied Materials & Interfaces*, 2016. **8**(51): p. 35219-35226.
80. Pattini, F., et al., Role of the substrates in the ribbon orientation of Sb₂Se₃ films grown by Low-Temperature Pulsed Electron Deposition. *Solar Energy Materials and Solar Cells*, 2020. **218**: p. 110724.
81. Oyeleke, O.D., et al., Absorption, diffraction and free space path losses modeling for the terahertz band. *Int. J. Eng. Manuf*, 2020. **10**: p. 54.
82. McMeeking, G., et al., Impacts of nonrefractory material on light absorption by aerosols emitted from biomass burning. *Journal of Geophysical Research: Atmospheres*, 2014. **119**(21): p. 12,272-12,286.
83. Kirchartz, T. and U. Rau, What makes a good solar cell? *Advanced energy materials*, 2018. **8**(28): p. 1703385.

84. Dhankhar, M., O.P. Singh, and V. Singh, Physical principles of losses in thin film solar cells and efficiency enhancement methods. *Renewable and Sustainable Energy Reviews*, 2014. **40**: p. 214-223.
85. Shiel, H., et al., Natural band alignments and band offsets of Sb₂Se₃ solar cells. *ACS Applied Energy Materials*, 2020. **3**(12): p. 11617-11626.
86. Ansari, M.I.H., A. Qurashi, and M.K. Nazeeruddin, Frontiers, opportunities, and challenges in perovskite solar cells: A critical review. *Journal of Photochemistry and Photobiology C: Photochemistry Reviews*, 2018. **35**: p. 1-24.
87. Urieta-Mora, J., et al., Hole transporting materials for perovskite solar cells: a chemical approach. *Chemical Society Reviews*, 2018. **47**(23): p. 8541-8571.
88. Ehtesham, A., et al., Recent Advances in Fabrication Techniques of Perovskite Solar Cells: A Review. *American Journal of Applied Sciences*, 2016. **13**(11): p. 1290-1314.
89. Han, D., et al., Ion implantation-modified fluorine-doped tin oxide by zirconium with continuously tunable work function and its application in perovskite solar cells. *ACS applied materials & interfaces*, 2017. **9**(48): p. 42029-42034.
90. Pan, Y., et al., Vapor transport deposition of highly efficient Sb₂(S, Se)₃ solar cells via controllable orientation growth. *Advanced Functional Materials*, 2021. **31**(28): p. 2101476.
91. Huang, J., et al., Improving the efficiency and stability of inverted perovskite solar cells with dopamine-copolymerized PEDOT: PSS as a hole extraction layer. *Journal of Materials Chemistry A*, 2017. **5**(26): p. 13817-13822.
92. Shi, W.-J., et al., Antimony Selenide Thin Film Solar Cells with an Electron Transport Layer of Alq₃. *Chinese Physics Letters*, 2020. **37**(10): p. 108401.
93. Escorcia-García, J., et al., Heterojunction CdS/Sb₂S₃ solar cells using antimony sulfide thin films prepared by thermal evaporation. *Thin Solid Films*, 2014. **569**: p. 28-34.
94. Yuan, S., et al., Efficient planar antimony sulfide thin film photovoltaics with large grain and preferential growth. *Solar Energy Materials and Solar Cells*, 2016. **157**: p. 887-893.

95. Yuan, S., et al., Postsurface selenization for high performance Sb₂S₃ planar thin film solar cells. *Acs Photonics*, 2017. **4**(11): p. 2862-2870.
96. Elsmami, M.I., et al., Recent issues and configuration factors in perovskite-silicon tandem solar cells towards large scaling production. *Nanomaterials*, 2021. **11**(12): p. 3186.
97. Ishaq, M., et al., Efficient copper-doped antimony sulfide thin-film solar cells via coevaporation method. *Solar RRL*, 2019. **3**(12): p. 1900305.
98. Zeng, Y., et al., Quasi-vertically-orientated antimony sulfide inorganic thin-film solar cells achieved by vapor transport deposition. *ACS applied materials & interfaces*, 2020. **12**(20): p. 22825-22834.
99. Kim, D.-H., et al., Highly reproducible planar Sb₂S₃-sensitized solar cells based on atomic layer deposition. *Nanoscale*, 2014. **6**(23): p. 14549-14554.
100. Lei, H., et al., Efficient planar Sb₂S₃ solar cells using a low-temperature solution-processed tin oxide electron conductor. *Physical Chemistry Chemical Physics*, 2016. **18**(24): p. 16436-16443.
101. Wang, X., et al., A fast chemical approach towards Sb₂S₃ film with a large grain size for high-performance planar heterojunction solar cells. *Nanoscale*, 2017. **9**(10): p. 3386-3390.
102. Tang, R., et al., n-type doping of Sb₂S₃ light-harvesting films enabling high-efficiency planar heterojunction solar cells. *ACS applied materials & interfaces*, 2018. **10**(36): p. 30314-30321.
103. Guo, C., et al., Enhanced electrical conductivity of Sb₂S₃ thin film via C60 modification and improvement in solar cell efficiency. *Global Challenges*, 2019. **3**(7): p. 1800108.
104. Cerdán-Pasarán, A., et al., Effect of cobalt doping on the device properties of Sb₂S₃-sensitized TiO₂ solar cells. *Solar Energy*, 2019. **183**: p. 697-703.
105. Gong, J., J. Liang, and K. Sumathy, Review on dye-sensitized solar cells (DSSCs): Fundamental concepts and novel materials. *Renewable and Sustainable Energy Reviews*, 2012. **16**(8): p. 5848-5860.
106. Wang, Y., S. Ji, and B. Shin, Interface engineering of antimony selenide solar cells: a review on the optimization of energy band alignments. *Journal of Physics: Energy*, 2022.

107. Tang, S., et al., Harnessing hierarchical architectures to trap light for efficient photoelectrochemical cells. *Energy & Environmental Science*, 2020. **13**(3): p. 660-684.
108. Zhao, B., et al., Efficient Sb₂Se₃ sensitized solar cells prepared through a facile SILAR process and improved performance by interface modification. *Applied Surface Science*, 2018. **450**: p. 228-235.
109. Taherinejad, M., Characterization of topological insulators and semiconductors. 2015: Rutgers The State University of New Jersey, School of Graduate Studies.
110. Wang, C., et al., Efficiency improvement of flexible Sb₂Se₃ solar cells with non-toxic buffer layer via interface engineering. *Nano Energy*, 2020. **71**: p. 104577.
111. Li, D.-B., et al., Stable and efficient CdS/Sb₂Se₃ solar cells prepared by scalable close space sublimation. *Nano Energy*, 2018. **49**: p. 346-353.
112. Wen, X., et al., Vapor transport deposition of antimony selenide thin film solar cells with 7.6% efficiency. *Nature communications*, 2018. **9**(1): p. 1-10.
113. Xu, Y., et al., Template deposition of Sb₂S₃ for solid-state sensitized solar cells. *Journal of Alloys and Compounds*, 2019. **784**: p. 947-953.
114. Itzhaik, Y., et al., Sb₂S₃-sensitized nanoporous TiO₂ solar cells. *The Journal of Physical Chemistry C*, 2009. **113**(11): p. 4254-4256.
115. Chen, C. and J. Tang, Open-circuit voltage loss of antimony chalcogenide solar cells: status, origin, and possible solutions. *ACS Energy Letters*, 2020. **5**(7): p. 2294-2304.
116. Chang, J.A., et al., High-performance nanostructured inorganic–organic heterojunction solar cells. *Nano letters*, 2010. **10**(7): p. 2609-2612.
117. Im, S.H., et al., Toward interaction of sensitizer and functional moieties in hole-transporting materials for efficient semiconductor-sensitized solar cells. *Nano letters*, 2011. **11**(11): p. 4789-4793.
118. Choi, Y.C., et al., Sb₂Se₃-sensitized inorganic–organic heterojunction solar cells fabricated using a single-source precursor. *Angewandte Chemie*, 2014. **126**(5): p. 1353-1357.

119. Messina, S., M. Nair, and P. Nair, Antimony selenide absorber thin films in all-chemically deposited solar cells. *Journal of the Electrochemical Society*, 2009. **156**(5): p. H327.
120. Leng, M., et al., Selenization of Sb₂Se₃ absorber layer: an efficient step to improve device performance of CdS/Sb₂Se₃ solar cells. *Applied Physics Letters*, 2014. **105**(8): p. 083905.
121. Zhou, Y., et al., Thin-film Sb₂Se₃ photovoltaics with oriented one-dimensional ribbons and benign grain boundaries. *Nature Photonics*, 2015. **9**(6): p. 409-415.
122. Tang, R., et al., Hydrothermal deposition of antimony selenosulfide thin films enables solar cells with 10% efficiency. *Nature Energy*, 2020. **5**(8): p. 587-595.
123. Wang, X., et al., Manipulating the electrical properties of Sb₂(S, Se)₃ film for high-efficiency solar cell. *Advanced Energy Materials*, 2020. **10**(40): p. 2002341.
124. Dong, J., et al., Boosting VOC of antimony chalcogenide solar cells: A review on interfaces and defects. *Nano Select*, 2021. **2**(10): p. 1818-1848.
125. Zhao, F., et al., Materials for solar-powered water evaporation. *Nature Reviews Materials*, 2020. **5**(5): p. 388-401.
126. Grosjean, A. and E. Le Baron, Longtime solar performance estimations of low-E glass depending on local atmospheric conditions. *Solar Energy Materials and Solar Cells*, 2022. **240**: p. 111730.
127. ELBASHAR, Y., et al., Glass Technology and Its Application in Solar Cells. *Nonlinear Optics, Quantum Optics: Concepts in Modern Optics*, 2021. **53**.
128. Sze, S.M., Y. Li, and K.K. Ng, *Physics of semiconductor devices*. 2021: John wiley & sons.
129. Chen, Z. and G. Chen, The effect of absorber thickness on the planar Sb₂S₃ thin film solar cell: Trade-off between light absorption and charge separation. *Solar Energy*, 2020. **201**: p. 323-329.
130. Sun, P.-P., et al., A new carbon phase with direct bandgap and high carrier mobility as electron transport material for perovskite solar cells. *npj Computational Materials*, 2019. **5**(1): p. 9.

131. Eke, M.N., Photovoltaic Characteristics and Applications, in *Electrode Materials for Energy Storage and Conversion*. 2021, CRC Press. p. 351-364.
132. Scappucci, G., et al., The germanium quantum information route. *Nature Reviews Materials*, 2021. **6**(10): p. 926-943.
133. Jia, Z., et al., High performance tandem organic solar cells via a strongly infrared-absorbing narrow bandgap acceptor. *Nature Communications*, 2021. **12**(1): p. 178.
134. Zhang, G., et al., Internal short circuit mechanisms, experimental approaches and detection methods of lithium-ion batteries for electric vehicles: A review. *Renewable and Sustainable Energy Reviews*, 2021. **141**: p. 110790.
135. Xiong, R., et al., Research progress, challenges and prospects of fault diagnosis on battery system of electric vehicles. *Applied Energy*, 2020. **279**: p. 115855.
136. Omatola, K. and V. Sule, An Experimental Analysis of Illumination Intensity and Tilt Angle Dependency of Photovoltaic Cell Electric Output Parameters. *Int. J. Sci. Res. in Physics and Applied Sciences Vol*, 2020. **8**(2).
137. Wong, J., et al., A systematic loss analysis method for rear-passivated silicon solar cells. *IEEE Journal of Photovoltaics*, 2015. **5**(2): p. 619-626.
138. El-Ahmar, M., A.-H.M. El-Sayed, and A. Hemeida. Mathematical modeling of Photovoltaic module and evaluate the effect of various parameters on its performance. in *2016 Eighteenth International Middle East Power Systems Conference (MEPCON)*. 2016. IEEE.
139. Sharma, D., R. Mehra, and B. Raj, *Design and Analysis of Various Solar Cell Technologies for Improvements in Efficiencies: A Review*. 2021.
140. Hsu, T.-W., et al., Photovoltaic energy harvester with fractional open-circuit voltage based maximum power point tracking circuit. *IEEE Transactions on Circuits and Systems II: Express Briefs*, 2018. **66**(2): p. 257-261.
141. Mohammadi, F., Design, analysis, and electrification of a solar-powered electric vehicle. *Journal of Solar Energy Research*, 2018. **3**(4): p. 293-299.
142. Alicki, R., D. Gelbwaser-Klimovsky, and A. Jenkins, A thermodynamic cycle for the solar cell. *Annals of Physics*, 2017. **378**: p. 71-87.

143. Klugmann-Radziemska, E. and P. Wcisło-Kucharek, Photovoltaic module temperature stabilization with the use of phase change materials. *Solar Energy*, 2017. **150**: p. 538-545.
144. Kurtuldu, S.H., Sb₂Se₃ absorber layered solar cell fabrication and characterization. 2021, Izmir Institute of Technology.
145. Nelson, J.A., *The physics of solar cells*. 2003: World Scientific Publishing Company.
146. Jayawardana, I.D., et al., A fast-dynamic control scheme for a power-electronics-based PV emulator. *IEEE Journal of Photovoltaics*, 2020. **11**(2): p. 485-495.
147. Wang, H., et al., Thermodynamic analysis and optimization of photovoltaic/thermal hybrid hydrogen generation system based on complementary combination of photovoltaic cells and proton exchange membrane electrolyzer. *Energy conversion and management*, 2019. **183**: p. 97-108.
148. Halme, J. and P. Mäkinen, Theoretical efficiency limits of ideal coloured opaque photovoltaics. *Energy & Environmental Science*, 2019. **12**(4): p. 1274-1285.
149. De la Mora, M., et al., Materials for downconversion in solar cells: Perspectives and challenges. *Solar Energy Materials and Solar Cells*, 2017. **165**: p. 59-71.
150. Soga, T., *Nanostructured materials for solar energy conversion*. 2006: Elsevier.
151. Mostefaoui, M., et al., Simulation of high efficiency CIGS solar cells with SCAPS-1D software. *Energy Procedia*, 2015. **74**: p. 736-744.
152. Sunny, A. and S.R.A. Ahmed, Numerical simulation and performance evaluation of highly efficient Sb₂Se₃ solar cell with tin sulfide as hole transport layer. *physica status solidi (b)*, 2021. **258**(7): p. 2000630.
153. Chen, C., et al., Characterization of basic physical properties of Sb₂Se₃ and its relevance for photovoltaics. *Frontiers of Optoelectronics*, 2017. **10**(1): p. 18-30.

154. Yin, B., et al., Buffer layer of PEDOT: PSS/graphene composite for polymer solar cells. *Journal of nanoscience and nanotechnology*, 2010. **10**(3): p. 1934-1938.
155. Chowdhury, M., et al., Effect of deep-level defect density of the absorber layer and n/i interface in perovskite solar cells by SCAPS-1D. *Results in Physics*, 2020. **16**: p. 102839.
156. Li, Z.-Q., M. Ni, and X.-D. Feng, Simulation of the Sb₂Se₃ solar cell with a hole transport layer. *Materials Research Express*, 2020. **7**(1): p. 016416.
157. Zyoud, S.H., et al., Numerical Modelling Analysis for Carrier Concentration Level Optimization of CdTe Heterojunction Thin Film–Based Solar Cell with Different Non–Toxic Metal Chalcogenide Buffer Layers Replacements: Using SCAPS–1D Software. *Crystals*, 2021. **11**(12): p. 1454.
158. Singh, R., et al., Review of current progress in inorganic hole-transport materials for perovskite solar cells. *Applied Materials Today*, 2019. **14**: p. 175-200.
159. Minbashi, M., et al., Simulation of high efficiency SnS-based solar cells with SCAPS. *solar energy*, 2018. **176**: p. 520-525.
160. Konstantakou, M. and T. Stergiopoulos, A critical review on tin halide perovskite solar cells. *Journal of Materials Chemistry A*, 2017. **5**(23): p. 11518-11549.
161. Lin, L.-y., et al., Analysis of Sb₂Se₃/CdS based photovoltaic cell: a numerical simulation approach. *Journal of Physics and Chemistry of Solids*, 2018. **122**: p. 19-24.
162. Xiao, Y., H. Wang, and H. Kuang, Numerical simulation and performance optimization of Sb₂S₃ solar cell with a hole transport layer. *Optical Materials*, 2020. **108**: p. 110414.
163. Burgelman, M., et al., Modeling thin-film PV devices. *Progress in Photovoltaics: Research and Applications*, 2004. **12**(2-3): p. 143-153.
164. Kao, K.C., *Dielectric phenomena in solids*. 2004: Elsevier.
165. Sridharan, A., et al., Time-resolved imaging of non-diffusive carrier transport in long-lifetime halide perovskite thin films. *arXiv preprint arXiv:1905.11242*, 2019.

166. Correa-Baena, J.-P., et al., Changes from bulk to surface recombination mechanisms between pristine and cycled perovskite solar cells. *ACS Energy Letters*, 2017. **2**(3): p. 681-688.
167. Abdulghani, Z.R., et al., Numerical simulation of quantum dots as a buffer layer in CIGS solar cells: a comparative study. *Scientific Reports*, 2022. **12**(1): p. 1-16.
168. Alam, I. and M.A. Ashraf, Effect of different device parameters on tin-based perovskite solar cell coupled with In₂S₃ electron transport layer and CuSCN and Spiro-OMeTAD alternative hole transport layers for high-efficiency performance. *Energy Sources, Part A: Recovery, Utilization, and Environmental Effects*, 2020: p. 1-17.
169. Ouslimane, T., et al., Impact of absorber layer thickness, defect density, and operating temperature on the performance of MAPbI₃ solar cells based on ZnO electron transporting material. *Heliyon*, 2021. **7**(3): p. e06379.
170. Jamal, M., et al., Effect of defect density and energy level mismatch on the performance of perovskite solar cells by numerical simulation. *Optik*, 2019. **182**: p. 1204-1210.
171. Smita, S., et al., Incorporation of phase changing materials (PCMs) with solar cells. 2022.
172. El-Wahabb, E.A., S. Fouad, and M. Fadel, Theoretical and experimental study of the conduction mechanism in Sb₂Se₃ alloy. *Journal of materials science*, 2003. **38**(3): p. 527-532.

VITAE

Name Saraswati Bajgai

Student ID 6310920019

Educational Attainment

| Degree | Name of Institution | Year of Graduation |
|---------------------------------------|---|--------------------|
| Bachelor of Science (Life Science) | Sherubtse College, Royal University of Bhutan | 2016 |

Scholarship Awards during Enrolment

1. Interdisciplinary Graduate School of Energy System Scholarship, Prince of Songkla University, Hat Yai, Thailand
2. Education fee grant, Discipline of Sustainable Energy Development , Faculty of Environmental Management, Prince of Songkla University, Hat Yai, Thailand.

List of Publications and Proceeding

Numerical Simulation of the Performance of Sb_2Se_3 Solar Cell via Optimizing the Optoelectronic Properties Based SCAPS-1D (2022)

Effect of KOH concentration on the properties of ZnO nanoparticles (2022)

Comparative studies on the morphological, structural, and optical properties of NiO thin films grown by vacuum and non-vacuum deposition techniques (2021)